Suppression of an Already Established Tumor Growing through Activated Mucosal CTLs Induced by Oral Administration of Tumor Antigen with Cholera Toxin[1]

Ayako Wakabayashi, Yohko Nakagawa, Masumi Shimizu, Keiichi Moriya, Yasuhiro Nishiyama, and Hidemi Takahashi[2]

Priming of CTLs at mucosal sites, where various tumors are originated, seems critical for controlling tumors. In the present study, the effect of the oral administration of OVA plus adjuvant cholera toxin (CT) on the induction of Ag-specific mucosal CTLs as well as their effect on tumor regression was investigated. Although OVA-specific TCRs expressing lymphocytes requiring in vitro restimulation to gain specific cytotoxicity could be detected by OVA peptide-bearing tetramers in both freshly isolated intraepithelial lymphocytes and spleen cells when OVA was orally administered CT, those showing direct cytotoxic activity without requiring in vitro restimulation were dominantly observed in intraepithelial lymphocytes. The magnitude of such direct cytotoxicity at mucosal sites was drastically enhanced after the second oral administration of OVA with intact whole CT but not with its subcomponent, an A subunit (CTA) or a B subunit (CTB). When OVA plus CT were orally administrated to C57BL/6 mice bearing OVA-expressing syngeneic tumor cells, E.G7-OVA, in either gastric tissue or the dermis, tumor growth was significantly suppressed after the second oral treatment; however, s.c. or i.p. injection of OVA plus CT did not show any remarkable suppression. Those mucosal OVA-specific CTLs having direct cytotoxicity expressed CD8$\alpha\beta$ but not CD8$\alpha\alpha$, suggesting that they originated from thymus-educated cells. Moreover, the infiltration of such OVA-specific CD8$^+$ CTLs was observed in suppressed tumor tissues. These results indicate that the growth of ongoing tumor cells can be suppressed by activated CD8$\alpha\beta$ CTLs with tumor-specific cytotoxicity via an orally administered tumor Ag with a suitable mucosal adjuvant. *The Journal of Immunology*, 2008, 180: 4000–4010.

Many malignant tumors originate from various epithelial tissues such as the skin or mucosal sites such as the esophagus, stomach, colon, or lung (1). Thus, as a cancer vaccine, it is essential to stimulate mucosal or dermal immune systems, as well as the systemic immune system, with a suitable Ag, adjuvant, and administration route as reviewed by Finn (2). Mucosal immunization using an adjuvant that enables the priming of both mucosal and systemic immunity (3, 4) may be a good way to prevent or treat mucosal tumors. In particular, the induction of mucosal CTLs that can specifically recognize tumor-derived peptide Ags presented by the corresponding class I MHC molecules seems to be one of the most important issues for eliminating tumor cells (5).

In the mucosal compartment, lymphocytes located in the intestinal epithelium are almost exclusively T cells called intraepithelial lymphocytes (IELs)[3] (3). Such IELs are mostly CD8$^+$ T cells that are classified into three distinct populations: TCR$\alpha\beta^+$CD8$\alpha\beta^+$, TCR$\alpha\beta^+$CD8$\alpha\alpha^+$, and TCR$\gamma\delta^+$CD8$\alpha\alpha^+$ (6). IELs contain cytotoxic properties and specifically eliminate virus- or parasite-infected cells (7–9); however, although spontaneous cytotoxicity of human IELs against tumor cells has been reported (10, 11), their actual specificity on tumors is still unknown. Recently, we have reported (12) that a marked increase in the number of HIV-1-specific CD8$\alpha\beta$-positive T cells among IELs was observed in HIV-1-specific TCR transgenic (Tg) mice when they received intrarectal or i.p. administration of the recombinant vaccinia virus (rVV) expressing a known restricted CTL epitope, P18 (rVV-P18), which is restricted by H-2D^d-class I MHC molecules (13). Using H-2D^d/P18 tetramers, we could detect CD8-positive, P18-specific TCR-expressing T cells in freshly isolated IELs and splenic T cells of unchallenged naive Tg mice. Although those H-2D^d/P18 tetramer-positive CD8 T cells from naive Tg mice did not show any specific cytotoxicity, freshly isolated mucosal T cells bearing CD8$\alpha\beta$ but not CD8$\alpha\alpha$ from activated Tg mice with rVV-P18 represented P18-specific cytotoxicity against tumor cells expressing the epitope, and the magnitude of cytotoxicity was much stronger than that in activated splenic T cells (12). These results suggest that in vivo activated mucosal CD8$\alpha\beta$ CTLs with tumor-specific cytotoxicity may be critical for controlling tumors expressing the specific epitope in vivo rather than systemic splenic CTLs.

Cholera toxin (CT) derived from *Vibrio cholerae* is known as a potent mucosal adjuvant comprised of one toxic A subunit (CTA) with ADP-ribosyltransferase activity and five nontoxic B subunits (CTB) responsible for binding to monosialoganglioside (GM) 1 on the cell surface (14, 15). CT adjuvant helps to produce both systemic IgG and mucosal IgA (16) as well as to induce Ag-specific

Department of Microbiology and Immunology, Nippon Medical School, Tokyo, Japan

Received for publication April 13, 2007. Accepted for publication January 7, 2008.

The costs of publication of this article were defrayed in part by the payment of page charges. This article must therefore be hereby marked *advertisement* in accordance with 18 U.S.C. Section 1734 solely to indicate this fact.

[1] This work was supported in part by Grants-in-Aid for Young Scientists from the Japan Society for the Promotion of Sciences, from the Ministry of Education, Science, Sport, and Culture, from the Ministry of Health and Labor and Welfare, Japan, and from the Promotion and Mutual Aid Corporation for Private Schools of Japan.

[2] Address correspondence and reprint requests to Dr. Hidemi Takahashi, Department of Microbiology and Immunology, Nippon Medical School, 1-1-5 Sendagi, Bunkyo-ku, Tokyo 113-8602, Japan. E-mail address: htkuhkai@nms.ac.jp

[3] Abbreviations used in this paper: IEL, intraepithelial lymphocyte; CT, cholera toxin; CTA, CT A subunit (toxic); CTB, CT B subunit (nontoxic); DC, dendritic cell; GM, monosialoganglioside; *Hp*, *Helicobacter pylori*; LPL, lamina propria lymphocyte; MadCAM-1, mucosal addressin cell-adhesion molecule-1; OVA-CT, CT-conjugated OVA; PP, Peyer's patch; rVV, recombinant vaccinia virus; SC, spleen cell; Tg, transgenic; TIL, tumor-infiltrating lymphocyte.

$CD4^+$ T cell responses in the spleen, reflecting the systemic compartment, and in Peyer's patches (PPs), reflecting the mucosal compartment (17). In addition, it has been demonstrated (18) that OVA-specific CTLs could be primed in C57BL/6 mice following oral exposure to a combination of OVA with CT, and specific cytotoxic activity was detected from spleen cells (SCs) only when they were restimulated in vitro with irradiated OVA-expressing syngeneic tumor cells, E.G7-OVA, which are OVA gene-transfected EL4 thymoma cells (19, 20). Also, intranasal preimmunization with OVA peptide (SIINFEKL) plus CT primed similar OVA-specific CTLs in the spleen of C57BL/6 mice, and the immunized mice were protected from the development of transferred E.G7-OVA (21).

Moreover, it has been shown that adoptive transfer of naive $CD8^+$ OVA-specific OT-I T cells into E.G7-OVA tumor-bearing syngeneic mice did not inhibit tumor growth, although adoptive transfer of preactivated OT-I CTL in vitro inhibited tumor growth in a dose-dependent manner (22). Furthermore, it has recently been reported that vaccination with dendritic cells (DCs) prepulsed ex vivo with CT-conjugated OVA (OVA-CT) gave rise to OVA-specific splenic $CD8^+$ T cells that produced IFN-γ, were cytotoxic to E.G7-OVA cells in vivo, and rejected already established in vivo E.G7-OVA tumors associated with high numbers of tumor-infiltrating $CD8^+$ T cells (23), indicating that the elimination of previously established tumor cells might require the infiltration of tumor-specific activated $CD8^+$ CTLs.

In the present study, we found two distinct types of $CD8\alpha\beta$-positive T cells among freshly isolated lymphocytes expressing OVA-specific TCRs, which can be detected by OVA peptide-bearing tetramers. One is in an activated effector state with cytotoxic activity and the other is a resting state and may gain cytotoxicity when stimulated with an OVA epitope peptide in vitro. Based on the observations, we defined direct cytotoxicity as the former state, in which freshly isolated and unstimulated CD8 T cells had specific cytotoxicity. Therefore, by comparing systemic SCs, we asked whether OVA-specific cytotoxic activity could be observed among freshly isolated IELs in mice orally administered OVA plus CT and examined whether those activated CTLs would reject or suppress the growth of already established tumors. Consequently, we observed dominant $TCR\alpha\beta$ and $CD8\alpha\beta$ OVA-specific CTL activities in freshly isolated IELs rather than in SCs after the oral administration of OVA plus CT, and such mucosal CTL activities could be expanded after oral boosting. Moreover, the growth of E.G7-OVA inoculated into the stomach or the epidermis was significantly suppressed, accompanied by the expansion of activated mucosal CTLs, and the infiltration of such OVA-specific $CD8\alpha\beta^+$ CTLs was observed in suppressed dermal tumor tissues. These results indicate that the growth of ongoing tumor cells can be suppressed in vivo by activated $CD8\alpha\beta$ CTLs with tumor-specific cytotoxicity via an orally administered tumor Ag with a suitable mucosal adjuvant.

Materials and Methods

Mice

Six- to 8-wk-old female C57BL/6 ($H\text{-}2^b$) mice were purchased from Charles River Japan, maintained in microisolator cages under pathogen-free conditions, and fed autoclaved laboratory chow and water. All animal experiments were performed according to guidelines for the care and use of laboratory animals set by the National Institutes of Health (NIH; Bethesda, MD) and approved by the Review Board of Nippon Medical School (Tokyo, Japan).

Oral and systemic immunization

Chicken egg OVA, grade V (Sigma Aldrich), was dissolved in sterilized PBS. Mice were orally administered 100 mg of OVA or 10 μg of CT (List Biological Laboratories) alone or 100 mg of OVA plus 10 μg of CT. CTA, or CTB (List Biological Laboratories) in 0.3 ml of PBS. In some experiments, mice were orally administered 10 mg of OVA plus 10 μg of CT. For systemic immunization, mice were i.p. or s.c. injected with 100 mg of OVA or the same dose of OVA plus 10 μg of CT.

Preparation of IELs, lamina propria lymphocytes (LPLs), SCs, and tumor-infiltrating lymphocytes (TILs)

IELs were prepared by the method described previously (12). In brief, after the small intestine, large intestine, or stomach was obtained from mice, fecal materials were flushed from the lumen with HBSS (Invitrogen Life Technologies) and connective tissues were carefully removed. The obtained guts were inverted and cut into several segments that were transferred to a 50-ml conical tube (Becton Dickinson Labware) containing 45 ml of HBSS with 5% FCS, 100 U/ml penicillin (Invitrogen Life Technologies), and 100 μg/ml streptomycin (Invitrogen Life Technologies). The tube was then shaken at 37°C for 45 min (horizontal position; orbital shaker at 150 rpm). Harvested cells from the intestinal epithelium were passed through a 10-ml syringe column containing loosely packed glass wool to remove tissue debris. Subsequently, the cells were suspended in 30% Percoll solution (Amersham Biosciences) and centrifuged for 20 min at 1,800 rpm. Cells at the bottom of the solution were then subjected to Percoll discontinuous gradient centrifugation for 20 min at 1,800 rpm and IELs were recovered at the interphase of 44 and 70% Percoll solutions. LPLs were prepared by the method described previously (24). In brief, after the small intestine, large intestine, or stomach was dissected from mice, fecal material was flushed from the lumen with HBSS and PPs were carefully removed. The obtained guts were inverted and cut into several segments that were transferred to a 50-ml conical tube containing 45 ml of HBSS with 5% FCS and 1 mM EDTA (Wako Pure Chemical Industries). The tube was shaken at 37°C for 45 min (horizontal position; orbital shaker at 150 rpm). The gut segments were then washed with PBS and shaken in 40 ml of HBSS with 5% FCS and 0.1 mg/ml collagenase (Sigma-Aldrich) at 37°C for 45 min (horizontal position; orbital shaker at 60 rpm). Harvested cells were passed through a nylon mesh and suspended in 40% Percoll solution, and then 70% Percoll solution was underlain. The solution was centrifuged for 20 min at 1,800 rpm and LPLs were recovered at the interphase of 40 and 70% Percoll solutions. These procedures provided >95% viable lymphocytes with a cell yield of $5\text{–}10 \times 10^6$ of small intestinal IELs, $2\text{–}3 \times 10^5$ of large intestinal IELs, $7\text{–}12 \times 10^3$ of gastric IELs, $4\text{–}9 \times 10^5$ of small intestinal LPLs, $1\text{–}3 \times 10^5$ of large intestinal LPLs, or $5\text{–}9 \times 10^4$ of gastric LPLs per mouse. The cells were suspended in complete T cell medium (25) composed of RPMI 1640 medium (Sigma-Aldrich) supplemented with 2 mM L-glutamine (ICN Biomedicals), 1 mM sodium pyruvate (Invitrogen Life Technologies), 0.1 mM nonessential amino acid (Invitrogen Life Technologies), a mixture of vitamins (ICN Biomedicals), 1 mM HEPES (Invitrogen Life Technologies), 100 U/ml penicillin (Invitrogen Life Technologies), 100 μg/ml streptomycin (Invitrogen Life Technologies), 50 μM 2-ME (Sigma-Aldrich), and heat-inactivated 10% FCS. For TIL preparation, tumors were removed from mice, incubated in 1 mg/ml collagenase (Wako Pure Chemical Industries) with PBS at 37°C for 1 h, and crushed gently. TILs were prepared using Percoll solutions as described in the previous paragraph regarding IEL preparation. The spleen was aseptically removed and a single cell suspension was prepared. For osmotic hemolysis, single cells were suspended in 0.1× PBS and an equal amount of 2× PBS was added immediately. To enrich IELs, LPLs, and TILs from mice, the interface between the 40 and 70% Percoll solutions (26), in which NK cells and unfractionated SCs, which may also include NK cells, must be included, was collected.

Flow cytometry analysis

Cells were double-stained with PE-labeled $H\text{-}2K^b$/OVA tetramer-SIINFEKL (Beckman Coulter) or $H\text{-}2K^b$/PB1 tetramer-SSYRRPVGI (Medical & Biological Laboratories) and FITC-labeled anti-mouse TCRβ, CD8α (BD Pharmingen), or CD8β (Caltag Laboratories). Peptide PB1 703–711, SSYRRPVGI, for the control tetramer was derived from influenza virus (27). Dead cells were determined using 7-aminoactinomycin D viability dye (Beckman Coulter) and stained cells were analyzed by FACScan using the CellQuest program (BD Biosciences).

In vitro restimulation of SCs or IELs with E.G7-OVA

Lymphocytes were restimulated in vitro by the method described previously (19). Freshly isolated SCs (3×10^7) or IELs (3×10^7) were restimulated with 3×10^6 irradiated (20,000 rad) E.G7-OVA cells (19, 20) ($H\text{-}2^b$; American Type Culture Collection) in 10 ml of complete T cell medium per upright 25-cm^2 flask in 5% CO_2 at 37°C for 6 days. Six days later, the viability of the lymphocytes was 35–51% in SCs and 16–26% in IELs. The

in vitro restimulated cells were collected and their OVA-specific cytotoxicity was measured by the following procedure.

CTL assay

For the CTL assay, freshly isolated IELs, SCs, or TILs were used. Cytolytic activity was measured using a standard ^{51}Cr-release assay as previously described (12). In brief, various numbers of effector cells were incubated with 3×10^3 ^{51}Cr-labeled targets for 6 h at 37°C in 200 μl of RPMI 1640 medium containing 10% FCS in round-bottom 96-well cell culture plates (BD Biosciences). After incubation, the plates were centrifuged for 10 min at 330 × *g*, and 100 μl of cell-free supernatants were collected to measure radioactivity with a Packard Auto-Gamma 5650 counter (Hewlett-Packard Japan). Maximum release was determined from the supernatant of cells that had been lysed by the addition of 5% Triton X-100, and spontaneous release was determined from target cells incubated without added effector cells. The percentage of specific lysis was calculated as 100 × (experimental release − spontaneous release)/(maximum release − spontaneous release). SEs of the means of triplicate cultures were always <5% of the mean. Each experiment was performed at least three times.

Measurement of in vivo antitumor effects

E.G7-OVA cells (5×10^6), OVA gene-transfected EL4 thymoma cells (19, 20), were implanted into the gastric or dermal tissue of syngeneic C57BL/6 mice (H-2^b). For tumor implantation into the gastric tissue, mice were anesthetized and underwent an abdominal operation and then E.G7-OVA cells in 50 μl of RPMI 1640 were injected into the muscle layer of the stomach using a syringe with a 29-gauge needle (Terumo). For implantation into the dermal tissue, mice were anesthetized and E.G7-OVA cells in 100 μl of RPMI 1640 were injected intradermally by a 29-gauge needle syringe. On day 3 after implantation into the gastric or dermal tissue, when the tumor mass became visible, tumor-bearing mice were orally or systemically administered OVA plus CT as described above. Seven days after the first administration, some of the mice were similarly boosted with the same materials. The growing tumors implanted into the gastric or dermal tissues were followed by measuring the length (*a*) and width (*b*), the and tumor volume (*V*) was calculated according to the formula $V = ab^2/2$ as reported previously (28). When the longer axis of each tumor was >20 mm, all mice were anesthetized and sacrificed according to the guidelines for the care and use of laboratory animals set by the NIH.

Histological analysis of tumor tissues

Freshly excised tumor tissues were embedded in Tissue-Tek OCT compound (Sakura Finetek) at −80°C. Tissue segments were sectioned at 6 μm using a cryostat. Sections were placed on a poly-L-lysine-coated glass slide, air dried, and then fixed in 10% formalin PBS for 5 min and stained with H&E. For immunohistochemical staining, sections were fixed in cold acetone for 5 min and incubated with blocking solution (Block-ace; Dainippon Pharmaceutical) for 30 min at 37°C and then incubated with biotin-conjugated rat anti-CD8β Ab (Caltag Laboratories) or control isotype-matched rat IgG2a Ab (Caltag Laboratories) overnight at 4°C. Endogenous peroxidase was quenched by incubation in 0.3% H_2O_2 and 0.1% NaN_3 in distilled water for 10 min. The sections were incubated with avidin-biotin peroxide complexes (Vectastain ABC kit; Vector Laboratories) followed by color reaction with a Vectastain diaminobenzidine substrate kit (Vector Laboratories).

Statistical analysis

Student's *t* test was used to determine the statistical significance of differences between groups in tumor growth. Data were considered significant at $p < 0.05$.

Results

Priming of OVA-specific CD8$\alpha\beta$-positive CTLs with direct cytotoxicity via oral administration with OVA plus CT

It has been reported that OVA-specific CTLs could be primed in C57BL/6 mice by oral or i.v. immunization with OVA plus CT together with nontoxic CTB, and specific cytotoxic activity was detected from immune SCs only when they were restimulated in vitro with irradiated OVA-expressing syngeneic tumor (E.G7-OVA) cells (18). It has also been shown that activated CTLs but not naive primed CTLs could represent antitumor responses in vivo (22). Similarly, we have recently observed in HIV-1-specific CTL-TCR transgenic mice that activated CTLs but not freshly isolated TCR-bearing CD8$\alpha\beta$-positive T cells showed specific cytotoxicity, and the most critical sites for activating TCR-bearing CD8$\alpha\beta$ T cells were mucosal compartments when Tg mice were administered a specific Ag for TCR (12).

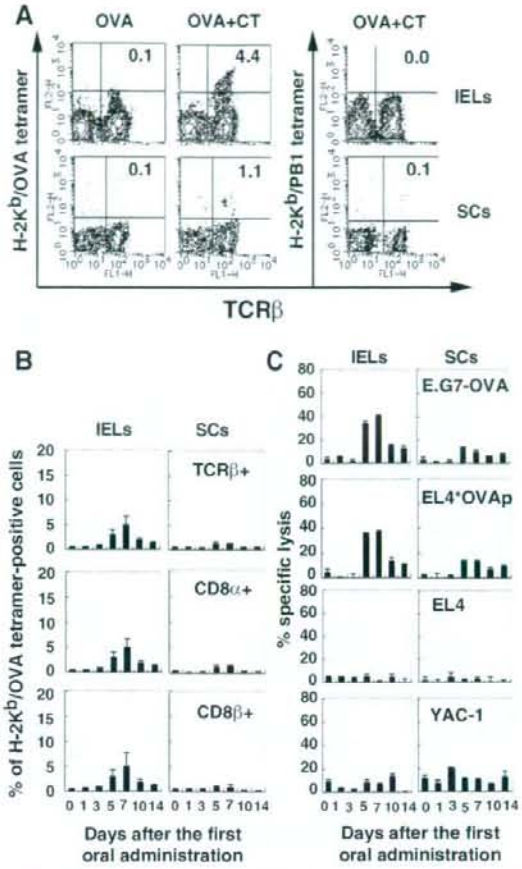

FIGURE 1. Analysis of OVA-specific direct cytotoxicities in IELs and SCs after primary immunization with OVA plus CT. *A*, Analysis of H-2K^b/OVA tetramer-positive cells. C57BL/6 mice were orally administered OVA or OVA plus CT once. IELs and SCs were collected from mice 5 days after the first oral administration, stained with either PE-labeled H-2K^b/OVA tetramer-SIINFEKL or H-2K^b/PB1 tetramer-SSYRRPVGI together with FITC-labeled anti-mouse TCRβ, and analyzed by flow cytometry. Each value represents the percentage of cells expressing both indicated markers. Data are representative of three independent experiments. *B*, Kinetics of H-2K^b/OVA tetramer-positive cells after primary immunization. C57BL/6 mice were orally administered OVA plus CT once. IELs and SCs were collected from mice at various days after the first oral administration, stained with PE-labeled H-2K^b/OVA tetramer together with FITC-labeled anti-mouse TCRβ, CD8α, or CD8β, and analyzed by flow cytometry. The results are shown as the mean ± SD of four mice. *C*, Kinetics of OVA-specific direct cytotoxic responses. C57BL/6 mice were orally primed and cells were collected as described in *B*. OVA-specific CTL responses were measured by ^{51}Cr-release assay using E.G7-OVA cells (H-2^b), YAC-1 cells, and EL4 cells (H-2^b) pulsed with or without 4 μM OVA-peptide, SIINFEKL, as target cells. E:T ratio was 100:1. The results shown as the mean ± SD in triplicate of pooled cells from two mice are representative of three independent experiments.

These findings prompted us to examine whether direct OVA-specific cytotoxic activity could be induced among IELs in mice

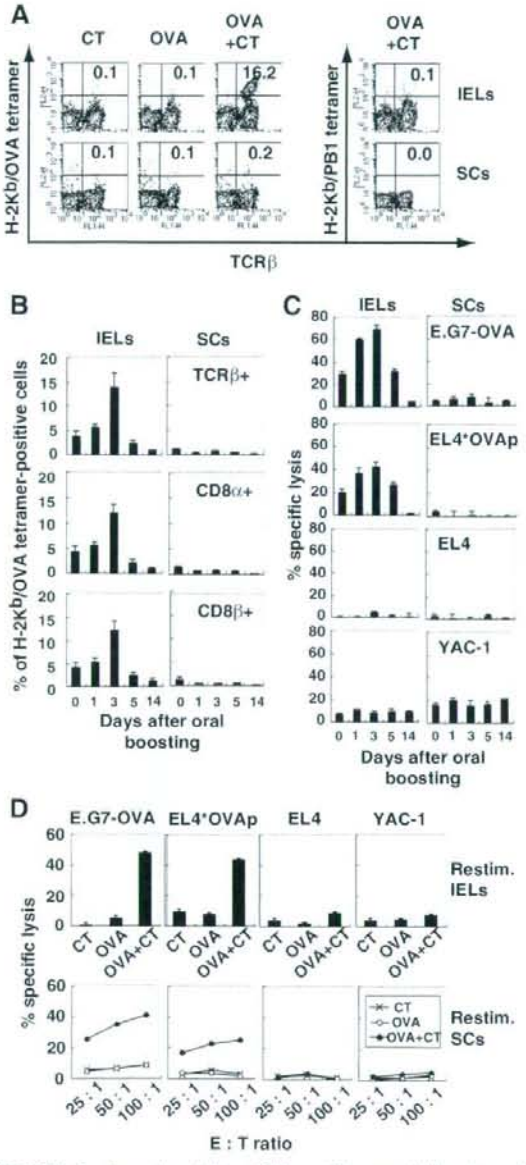

FIGURE 2. Expansion of direct OVA-specific cytotoxicities after oral boosting with OVA plus CT. *A*, Activated H-2K^b/OVA tetramer-positive cells after oral boosting. C57BL/6 mice were orally administered CT, OVA, or OVA plus CT once weekly for 2 wk. IELs and SCs were collected from mice 3 days after the second oral boost and stained with PE-labeled H-2K^b/OVA tetramer or H-2K^b/PB1 tetramer together with FITC-labeled anti-mouse TCRβ. Each value represents the percentage of cells expressing both indicated markers. Data are representative of three independent experiments. *B*, Kinetics of H-2K^b/OVA tetramer-positive cells after oral boosting. C57BL/6 mice were orally administered OVA plus CT once weekly for 2 wk. IELs and SCs were collected from mice at various days after the second oral boost, stained with PE-labeled H-2K^b/OVA tetramer together with FITC-labeled anti-mouse TCRβ, CD8α, or CD8β, and analyzed by flow cytometry. The results are shown as the mean ± SD of four mice. *C*, Kinetics of the secondary expansion of OVA-specific direct CTL responses. C57BL/6 mice were treated orally and the cells were collected as described in *B*. OVA-specific CTL responses were measured by ^{51}Cr-release assay using E.G7-OVA cells, YAC-1 cells, and EL4 cells pulsed with or without OVA peptide as targets. The E:T ratio is 100:1. The results shown as the mean ± SD in triplicate of pooled cells from two mice are representative of three independent experiments. *D*, Activation of OVA-specific CTLs by in vitro restimulation (Restim.). C57BL/6 mice were orally administered CT, OVA, or OVA plus CT once weekly for 2 wk. IELs (3×10^7) and SCs (3×10^7) were collected from mice 9 days after the second oral boost, and cocultured with 3×10^6 irradiated E.G7-OVA. Six days later, OVA-specific lysis of stimulated IELs and SCs was measured by ^{51}Cr-release assay. The E:T ratio is 100:1 in IELs and 100:1, 50:1, or 25:1 in SCs. The results are shown as the mean ± SD in IELs or the mean in SCs in triplicate of pooled cells from two mice. Data are representative of three independent experiments.

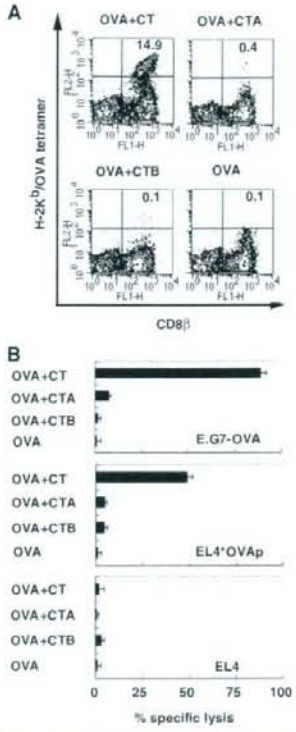

FIGURE 3. Both subunits, CTA and CTB, are essential for the induction of OVA-specific CTLs. C57BL/6 mice were orally administered OVA or OVA plus intact CT, CTA subunit or CTB subunit once weekly for 2 wk. IELs were collected from mice 3 days after the second oral administration. *A*, IELs were stained with PE-labeled H-2K^b/OVA tetramer and FITC-labeled anti-mouse CD8β. Each value represents the percentage of cells expressing both indicated markers. *B*, OVA-specific CTL responses of isolated IELs were measured by ^{51}Cr-release assay using E.G7-OVA cells, EL4 cells pulsed with or without OVA peptide as targets. The E:T ratio is 100:1. Data are shown as the mean ± SD in triplicate of pooled cells from two mice. The results are representative of three independent experiments for both *A* and *B*.

administered OVA plus CT orally without requiring in vitro restimulation. To carry out this experiment, we used a H-2K^b/OVA tetramer to detect cells expressing OVA-specific TCR in freshly isolated IELs as well as in the SCs of primed mice 5 days after immunization. Also, to evaluate the purity of IELs, CD103 (integrin

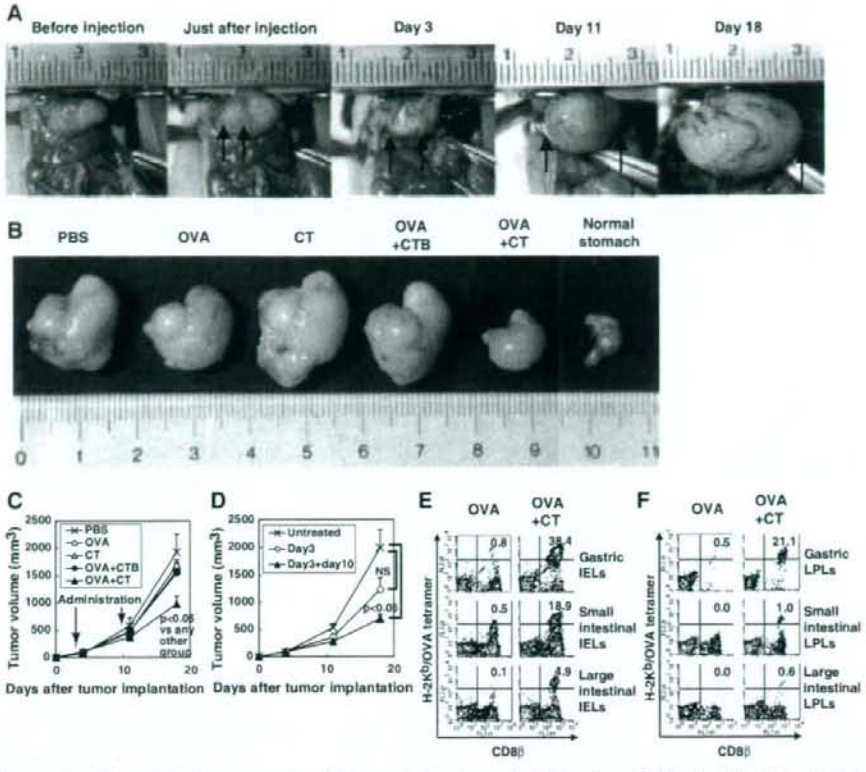

FIGURE 4. Suppression of the growth of a tumor implanted into gastric tissue by oral administration of OVA plus CT. *A*, Growth of visible tumor after implantation of E.G7-OVA cells into gastric tissue. C57BL/6 mice were implanted with 5×10^6 E.G7-OVA cells into the muscle layer of the stomach. Each day, the same mice were anesthetized and underwent an abdominal operation, and tumors were observed. Arrows point to both ends of the longer axis in the tumor. *B*, C57BL/6 mice were implanted with 5×10^6 E.G7-OVA cells into the muscle layer of the stomach. Three days later, tumor-bearing mice were orally administered PBS, OVA, CT, OVA plus CTB subunit, or OVA plus CT. Seven days later, the second oral administration was performed in the same manner. Stomachs were excised from the mice 18 days after tumor implantation, as well as from untreated, normal mice. *C*, Tumor volumes were calculated based on the formula described in *Materials and Methods*, and the results are shown as the mean ± SEM. The results were obtained from 9–13 mice per group. $p < 0.05$ indicates statistically significant difference between OVA plus CT (▲) and any other groups. *D*, C57BL/6 mice were implanted with E.G7-OVA cells in the stomach. Three days later, tumor-bearing mice were orally administered OVA plus CT or left untreated. Seven days later, some orally immunized mice were boosted in the same manner or left untreated. The results are shown as the mean ± SEM of 5–7 mice per group. $p < 0.05$ and NS indicate statistically significant and not significant differences, respectively, between the boosted (▲) and nonboosted (○) groups and the untreated group (×). *E* and *F*, Induction of CD8β and H-2K^b/OVA tetramer-positive cells in IELs (*E*) and LPLs (*F*) of the stomach, small intestine, or large intestine after oral administration of OVA plus CT. C57BL/6 mice were orally administered OVA or OVA plus CT once weekly for 2 wk. IELs and LPLs were collected from mice 3 days after the second oral administration. Cells were stained with PE-labeled H-2K^b/OVA tetramer and FITC-labeled anti-mouse CD8β. Each value represents the percentage of cells expressing both indicated markers. The results are representative of three independent experiments.

α-IEL chain)-positive cells in the collected samples were examined by flow cytometry. CD103 is highly expressed on >90% of IELs (29, 30) but on only 15% of SCs (31). In the present study, CD103-positive cells occupied >90% of IELs and ~15% of SCs (data not shown). Although a small number of OVA-specific TCR-expressing cells were detected in both IELs (4.5–5.0%) and SCs (1.0–1.5%) after oral administration of OVA plus CT in comparison with control H-2K^b/PB1-positive cells, H-2K^b/OVA tetramer-positive cells were not observed in mice treated with OVA alone (Fig. 1*A*). Such OVA peptide-specific TCR-expressing cells were TCRγδ negative (data not shown) and both CD8α and β positive (Fig. 1*B*). The number of tetramer-positive cells, to which the magnitude of direct OVA-specific cytotoxicity closely corresponded, was maximal at day 7 after oral immunization with both IELs and SCs (Fig. 1*B*), but it did not correspond to NK cell activity as measured against YAC-1 targets (Fig. 1*C*). The results clearly demonstrate that direct OVA-specific CTL cytotoxicity is dominantly observed in mucosal IELs after primary oral administration of OVA plus CT.

Augmentation and kinetics of direct OVA-specific cytotoxicity by CD8αβ CTLs among IELs and SCs via oral boosting with OVA plus CT at day 7 after the primary administration

As shown above, because only 4.5–5.0% of IELs were temporarily activated by a one-shot oral administration, we extensively examined the effect of oral boosting with OVA plus CT at various days after primary immunization. The number of H-2K^b/OVA tetramer-positive cells was significantly enhanced among IELs but not among SCs when primed mice were boosted (Fig. 2*A*). Such an effect was highest when mice were boosted at day 7 after initial

priming (data not shown). Tetramer-positive cells were again TCRβ-, CD8α-, and CD8β-positive IELs and their number peaked at day 3 after boosting (Fig. 2*B*). Correspondingly, direct OVA-specific cytotoxicity was greatly enhanced among IELs and the maximal cytotoxicity of IELs was observed at day 3 after boosting (Fig. 2*C*), although such direct cytotoxicity appeared to be completely lost in SCs (Fig. 2*C*). Nonetheless, SCs showed good epitope-specific cytotoxicity similar to that of IELs when they were restimulated in vitro with irradiated E.G7-OVA (Fig. 2*D*), suggesting that the priming effect by the oral administration of OVA plus CT also remained in systemic SCs.

It should be noted that the memory of OVA-specific CTLs persisted among IELs but not SCs. When secondary boosting with OVA plus CT was performed even 6 mo after primary boosting at day 7, the number of H-2K^b/OVA tetramer-positive cells was still detected at ~6% in IELs, and they showed remarkable direct cytotoxicity of ~84.5% against E.G7-OVA cells and 58.4% against EL4 cells pulsed with OVA peptide 3 days after secondary boosting (data not shown). Again, we could not detect any measurable direct cytotoxicity in the SCs of secondary boosted mice (data not shown).

Both CTA and CTB subunits are required to induce direct OVA-specific cytotoxicity in IELs

CT is comprised of a single A subunit, CTA, and five B subunits, CTB. When OVA was administered orally to mice with either 10 μg of CTA or an equal amount of CTB, H-2K^b/OVA tetramer-positive cells as well as direct OVA-specific cytotoxicity could not be detected in IELs (Fig. 3, *A* and *B*) and SCs (data not shown), although a significant number of tetramer-positive cells and strong direct OVA-specific cytotoxicity were observed among IELs of mice administered orally with OVA plus 10 μg of intact CT (Fig. 3, *A* and *B*). Even when using 50 μg of CTA or CTB for the administration of OVA, direct cytotoxicity was not observed (data not shown); therefore, both CTA and CTB subunits are required to induce direct Ag-specific cytotoxicity.

Effects of oral administration and booting with OVA plus CT on OVA-expressing tumor growth established in the stomach

We then examined in vivo antitumor effects of oral administration with tumor Ag plus CT on already established tumors growing in mice. C57BL/6 mice were implanted with 5×10^6 syngeneic E.G7-OVA cells into the muscle layer of the stomach (Fig. 4*A*). Three days later, tumor-bearing mice (Fig. 4*A*) were orally administered various combinations of OVA plus adjuvant and boosted with the same materials 7 days after the initial oral administration. To our surprise, tumor growth in the stomach of mice orally administered OVA plus CT twice was visually (Fig. 4*B*) and significantly ($p < 0.05$; Fig. 4*C*) suppressed on day 18 after tumor implantation as compared with other control groups such as OVA plus CTB or CT alone. However, when tumor-bearing mice were orally administered OVA plus CT once and without boosting, no statistically significant suppression was observed on day 18 as compared with untreated control mice, although a slight suppressive effect could be seen (Fig. 4*D*). Therefore, two oral administrations of tumor-Ag plus CT with an appropriate interval induced significant ongoing tumor suppression.

As previously shown, direct OVA-specific cytotoxicity among small intestinal IELs was greatly enhanced after boosting with OVA plus CT (Fig. 2, *A*, *B*, and *C*). We also examined whether direct OVA-specific CTLs were induced in the IELs and LPLs of the stomach, small intestine, and large intestine from boosted mice in which gastric tumor growth was significantly suppressed. We observed an increase in the number of H-2K^b/OVA tetramer-positive

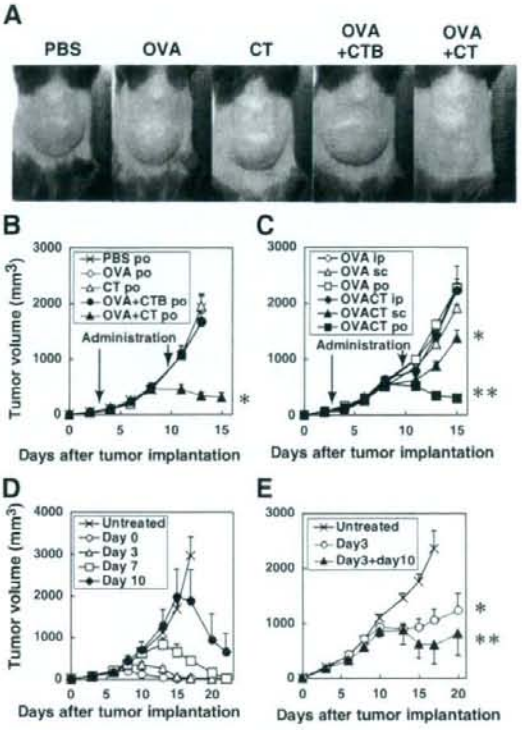

FIGURE 5. Suppression of intradermal tumor growth by oral administration with OVA plus CT. C57BL/6 mice were implanted intradermally with 5×10^6 E.G7-OVA cells. Three days later, tumor-bearing mice were orally administered PBS, OVA, CT, OVA plus CTB subunit, or OVA plus CT. Seven days later, the second oral administration was performed in the same manner. *A*, Visual suppressive effect of oral inoculation of OVA plus CT on dermal tumor growth. *B*, Tumor volumes were calculated based on the formula described in *Materials and Methods* and the results are shown as the mean ± SEM. Results were obtained from 5–6 mice per group. The asterisk (*) indicates statistically significant difference between the OVA plus CT group (closed triangle) and any other group at 11 days ($p < 0.05$) and 13 days ($p < 0.005$) after tumor inoculation. *C*, C57BL/6 mice were implanted intradermally with E.G7-OVA cells. Three days later, tumor-bearing mice were intraperitoneally (ip), subcutaneously (sc), or orally (po) administered OVA alone or OVA plus CT. Seven days later, the second treatment was performed in the same manner. The results are shown as the mean of tumor volumes ± SEM. Results were obtained from 5–6 mice per group. The asterisk (*) shows statistically significant differences ($p < 0.05$) between the s.c. OVA plus CT group (▲) and the s.c. OVA alone group at days 11, 13, and 15 after tumor implantation, and the two asterisks (**) indicate significant differences ($p < 0.01$) between the oral OVA plus CT group (■) and the oral OVA alone group on the same days. *D*, C57BL/6 mice were implanted intradermally with E.G7-OVA cells. The mice were orally administered once with OVA plus CT at day 0, 3, 7, or 10 after tumor implantation. The results are shown as the mean of tumor volumes ± SEM. Results were obtained from 10–12 mice per group. In single orally administered groups, significant tumor regression ($p < 0.05$) was observed at 7 days after oral administration compared with the untreated group. *E*, C57BL/6 mice were implanted intradermally with E.G7-OVA cells. Three days later, tumor-bearing mice were orally administered a low dose (10 mg) of OVA plus CT. Seven days later, some orally administered mice were boosted in the same manner. The results obtained from 5- mice per group are shown as the mean of tumor volumes ± SEM. The asterisk (*) indicates statistically significant differences ($p < 0.01$) between the nonboosted (○) and untreated mice (×) groups at days 15 and 17 after tumor implantation, and the two asterisks (**) indicate significant differences ($p < 0.005$) between the boosted (▲) and untreated groups on the same days.

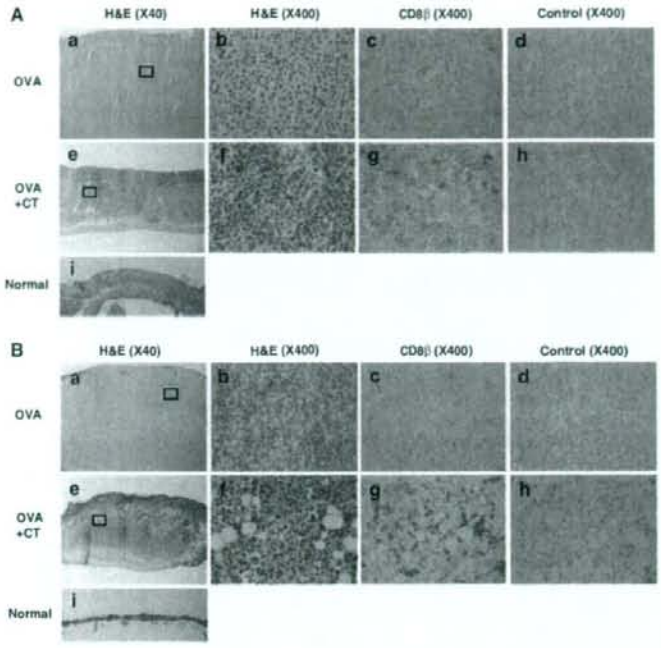

FIGURE 6. Infiltration of CD8$\alpha\beta$ positive lymphocytes into tumor tissues in mice orally administered OVA plus CT. C57BL/6 mice were implanted with 5×10^5 E.G7-OVA cells into the muscle layer of the stomach (*A*, *a–h*) or skin (*B*, *a–h*). Three days later, tumor-bearing mice were orally administered OVA (*A*, *a–d*, and *B*, *a–d*) or OVA plus CT (*A*, *e–h* and *B*, *e–h*). Seven days later, the second oral administration was performed in the same manner. Gastric and dermal tumor tissues were removed from mice 3 days after the second oral boost. Frozen sections of tumor tissues and normal tissues were prepared and stained with H&E (*A*, *a*, *b*, *e*, *f*, and *i* and *B*, *a*, *b*, *e*, *f*, and *i*) or immunohistochemically stained with biotin-conjugated rat anti-CD8β mAb (*A*, *c* and *g*, and *B*, *c* and *g*) or control isotype-matched rat IgG2a Ab (*A*, *d* and *h*, and *B*, *d* and *h*). Image magnification is either ×40 (*A*, *a*, *e*, and *i* and *B*, *a*, *e*, and *i*) or ×400 (*A*, *b–d* and *f–h* and *B*, *b–d* and *f–h*). *A*, *b* and *f* and *B*, *b* and *f* are enlarged images (×400) of the squared areas in the images (×40) of *A*, *a* and *e* and *B*, *a* and *e*, respectively.

cells among IELs in the stomach (38.4%) as well as the small (18.9%) and large intestine (4.9%) of tumor-suppressed mice (Fig. 4*E*) and also among LPLs in the stomach (21.1%) as well as the small (1.0%) and large (0.6%) intestine (Fig. 4*F*). Thus, the ability of LPLs to suppress tumor growth may be weaker than that of IELs. The results suggest that oral administration of Ag plus intact CT with appropriate mucosal boosting apparently suppressed the already established tumor growth in gastric tissue, particularly after oral boosting, probably through the activation of Ag-specific CTLs in the mucosal compartment.

Effects of oral administration and boosting with OVA plus CT on already established OVA-expressing dermal tumor growth

Next, we investigated the effect of the oral administration of tumor Ag plus CT on tumor growth in the skin, where the digestive tract is not directly associated. Mice were implanted with 5×10^5 E.G7-OVA cells intradermally. Three days later, tumor-bearing mice were orally administered various combinations of OVA plus adjuvant and boosted with the same materials 7 days after the initial oral administration. Interestingly, intradermal tumor growth was again strongly suppressed visually 11 days after tumor implantation in the dermis of mice orally administered OVA plus CT as compared with various other groups (Fig. 5*A*). This visual effect was confirmed by calculating the volume of the tumors established at day 11 and day 13 in each group ($p < 0.05$ and $p < 0.005$, respectively; Fig. 5*B*). We also examined the effect of the administration of tumor Ag plus CT via various routes on intradermal tumor growth. Although a slight suppression was observed by s.c. inoculation of OVA plus CT, tumor growth was not suppressed at all by i.p. administration in comparison with the oral treatment group (Fig. 5*C*). It should be noted that tumor growth in the dermis was markedly suppressed even by a single oral administration of OVA plus CT on day 0, 3, 7, or 10 after tumor implantation (Fig. 5*D*). In each group, tumor growth was suppressed ($p < 0.05$) and the tumor volume was small around 7 days after oral administration. Unexpectedly, there was almost no difference in the suppressive effects on tumor growth between mice treated with a single administration and boosted mice showing much stronger direct cytotoxicity (data not shown). However, when the dosage quantity of OVA was decreased by one-tenth, tumor growth in boosted mice was more significantly ($p < 0.005$) suppressed than in nonboosted mice ($p < 0.01$; Fig. 5*E*). Collectively, the results indicate that the oral administration of tumor Ag plus CT with appropriate mucosal boosting may induce a remarkable suppression of already established tumor growth in the skin via mucosally generated CTLs.

Infiltration of CD8$\alpha\beta$-positive cells in suppressed tumor tissues

We thus examined whether OVA-specific CD8$\alpha\beta$-positive CTLs were actually seen in suppressed tumor tissues such as the stomach and dermis. To determine tumor-infiltrating CD8$\alpha\beta^+$ cells, immunohistochemical staining was performed using biotin-conjugated rat anti-CD8β Ab (Fig. 6*A*, *c* and *g* and *B*, *c* and *g*) or control isotype-matched rat IgG2a Ab (Fig. 6*A*, *d* and *h* and *B*, *d* and *h*). Indeed, although mononuclear cells were seen in the gastric tumor tissues of mice treated with OVA alone, CD8$\alpha\beta$-positive cells were not observed at all (Fig. 6*A*, *a–d*). In contrast, infiltration of inflammatory mononuclear cells together with CD8$\alpha\beta$-positive cells was observed in suppressed gastric tumor tissues (Fig. 6*Ag*). As shown in Fig. 6*Ai*, normal gastric tissue is composed of the epithelium, lamina propria, lamina muscularis mucosae, muscle layer, and serosa from the inside surface in sequence. As compared with normal gastric tissue, a great number of large tumor cells (EG.7-OVA) were mainly found between the lamina muscularis mucosae and serosa of tumor-implanted tissues (Fig. 6*A*, *a* and *b*) and the infiltration of tumor cells into the lamina propria over the lamina muscularis mucosae was also observed (data not shown). However, in suppressed gastric tumor tissues (Fig. 6*Ae*) the tumor cell layer under the lamina muscularis mucosae was markedly thinner than that of an unsuppressed tumor (Fig. 6*Aa*), in which

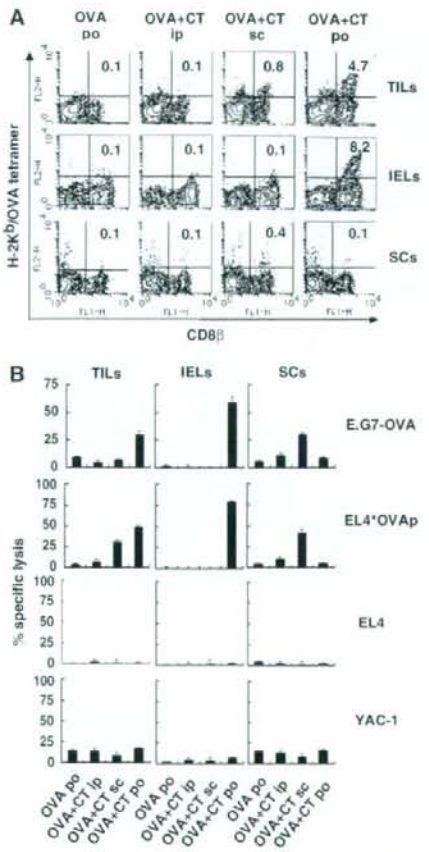

FIGURE 7. Detection of OVA-specific CTLs in TILs. C57BL/6 mice were implanted intradermally with E.G7-OVA cells. Three days later, mice were orally (po), subcutaneously (sc), or intraperitoneally (ip) administered OVA plus CT or orally treated with OVA. Seven days later, the second oral administration was performed in the same manner. TILs, IELs, and SCs were collected from mice 3 days after the second oral administration. *A*, TILs, IELs and SCs were double stained with PE-labeled H-2K^b/OVA tetramer and FITC-labeled anti-mouse CD8β. *B*, OVA-specific CTL responses of TILs, IELs, and SCs were measured by a ^{51}Cr-release assay using E.G7-OVA cells, YAC-1 cells, and EL4 cells pulsed with or without OVA peptide as targets. The E:T ratio is 5:1 in TILs, or 100:1 in IELs and SCs. The results are shown as the mean ± SD in triplicate of pooled cells from three mice. The results are representative of three independent experiments.

tumor cells almost never infiltrated the lamina propria over the lamina muscularis mucosae. Similarly, as for dermal tumor tissues, mononuclear cells together with CD8αβ-positive cells were not observed in mice treated with OVA alone (Fig. 6*B*, *a–d*), whereas the infiltration of a large number of mononuclear cells and CD8αβ-positive cells was observed in suppressed dermal tumor tissues (Fig. 6*B*, *e–g*). Dermal tumor sections were not stained with control isotype-matched rat IgG (Fig. 6*B*, *d* and *h*). As shown in Fig. 6*Bi*, normal skin is composed of epidermides and dermis from the surface in sequence. In tumor cell-implanted dermal tissues, although the infiltration of mononuclear cells or CD8αβ-positive cells was not observed, many large tumor cells were found thickly beneath the epidermides (Fig. 6*B*, *a* and *b*); however, when tumor cell-implanted mice were treated with OVA plus CT, most tumor cells became necrotic or apoptotic (Fig. 6*B*, *e* and *f*).

Measurement of tumor-specific cytotoxic activity by tumor-infiltrating cells in tumor-suppressed mice

To confirm whether infiltrated CD8αβ-positive T cells achieved OVA-specific cytotoxicity, we isolated TILs containing both mononuclear cells and CD8αβ-positive T cells from suppressed dermal tumor tissues as well as from their IELs and SCs. As expected, the number of H-2K^b/OVA tetramer-positive cells increased in both the TILs and IELs but not in the SCs of mice bearing suppressed tumors induced by oral administration with OVA plus CT as compared with mice inoculated with OVA plus CT via another route (Fig. 7*A*), and those increased tetramer-positive cells showed significant direct OVA-specific CTL activity (Fig. 7*B*). It should be noted that, although the number of increased cells specific for the H-2K^b/OVA tetramer was small in mice inoculated with OVA plus CT s.c., both the TILs (0.8%) and the SCs (0.4%) but not the IELs (0.1%) of the mice represented a detectable level of direct OVA-specific cytotoxicity (Fig. 7*B*). These findings suggest that s.c. immunization with Ag plus CT may preferably activate systemic (splenic) Ag-specific CTLs rather than local (intraepithelial) CTLs. Moreover, NK cell cytotoxicity determined against YAC-1 cells was not observed in TILs, IELs, and SCs by oral, s.c., or i.p. immunization of OVA plus CT (Fig. 7*B*), indicating that the suppression of tumor growth was mainly mediated by CD8αβ CTLs rather than by NK cell cytotoxicity.

Discussion

In the present study we demonstrated that when OVA plus intact CT was orally administered into mice, direct OVA-specific cytotoxicity was dominantly induced in IELs rather than SCs after the first oral priming, and direct OVA-specific cytotoxicity was remarkably expanded in IELs but not in SCs after oral boosting with the same doses of OVA plus CT. Such OVA-specific CTLs were thymic conventional K^b class I MHC molecule-restricted TCRαβ$^+$ CD8αβ T cells (32). Moreover, the growth of the OVA-expressing tumor E.G7-OVA thymoma, established previously either in the stomach or dermis, was significantly suppressed by the oral administration of OVA plus CT. Furthermore, marked infiltration of OVA-specific TCRαβ$^+$ CD8αβ CTLs with direct cytotoxicity in reduced tumor tissues was observed. These results suggest that activated CTLs with specific cytotoxicity generated at mucosal compartments by oral administration with OVA plus intact CT may be responsible for already established tumor regression.

The majority of tumor regression studies associated with activation of the immune system have focused on systemic immunity observed in the spleen, lymph nodes, and circulating blood rather than local mucosal immunity seen in gut IELs. Those studies have demonstrated only preventative results for tumor establishment by preadministration of tumor Ag plus a suitable adjuvant. In addition, to our knowledge only one study has been shown to suppress already established tumor growth by activating and expanding tumor infiltrating CD8$^+$ CTLs (23). In that study, i.v. vaccination with DCs prepulsed ex vivo with OVA-CT at day 3 and boosted at day 10 after OVA-expressing E.G7 tumor injection induced complete rejection of a visible tumor within 3 wk after the first treatment. Although the inoculation route and the materials for vaccination were different from ours, the timing of the priming and boosting to induce the suppression of already established tumor growth correlated exactly, suggesting that their methods may also initiate strong mucosal direct cytotoxicity mediated through CD8$^+$ CTLs.

Similar to our findings, they also showed that immunization with OVA-CT but not with CTB-conjugated OVA (OVA-CTB)-prepulsed DCs could successfully induce complete rejection of already established tumor growth, although OVA-CTB-prepulsed DC inoculation prevented tumor establishment but not ongoing tumor growth in the skin. Moreover, they insisted that OVA has to be coupled to CT and should be loaded onto DCs for therapeutic DC vaccination based on the observation that neither OVA-CT nor DCs pulsed with unconjugated OVA plus CT could prevent tumor progression. Nonetheless, our findings shown here apparently indicate that we were able to induce effective suppression of ongoing tumor growth by simple oral administration with unconjugated OVA and CT. These results suggest that we may control already established tumor growth at the surface compartments by activating mucosal $CD8^+$ CTLs via orally administered tumor Ag with a suitable mucosal adjuvant. Also, when OVA-CT is orally administered, the conjugation between OVA and CT may be broken through digestion by enzymes secreted in the gastrointestinal tract. Recently, we have reported that modification of OVA in the gastrointestinal tract is essential for oral tolerance induction against OVA (33). Therefore, it is possible that gastrointestinal digestion or modification of OVA may facilitate the delivery of OVA Ag into DCs, critical APCs for OVA-specific CTL induction.

For the efficient induction of such OVA-specific CTLs in vivo using DCs, Eriksson et al. have reported that OVA-CT-prepulsed DC immunization required at least two DC injections, reflecting the priming/boosting procedure (23); however, we have observed that a single oral administration of OVA plus CT seems sufficient to induce effective CTLs to prevent E.G7-OVA thymoma growth, particularly in the skin. This may be because mucosally activated CTLs through oral immunization may be more potent than systemically activated CTLs to suppress transplanted tumors at the mucosal compartment, and oral administration of OVA plus CT seems more efficient to induce mucosal CTLs than i.v. Ag-loaded DC inoculation. Further studies will be needed to explain the differences.

Although both CT-conjugated-OVA and CTB-conjugated OVA are cross-presented by MHC class I in DCs, only CT-OVA but not CTB-OVA cross-primes OVA-specific $CD8^+$ CTLs in vivo (23, 34). Additionally, DCs pulsed with intact OVA alone cannot cross-present and cross-prime CTLs (23). For the cross-priming of Ag-specific CTLs by Ag-captured immature DCs, maturation signaling via some surface molecules such as TLR-3 in those DCs is essential (35, 36). Although whole CT up-regulates the expression of MHC class II, B7.1, and B7.2 molecules on DCs in vitro, neither CTA nor CTB alone up-regulates the levels of surface markers on DCs (37, 38). Also, the binding of CTB to GM1 on DCs seems necessary to efficiently take up both CT itself and Ag and to induce cross-presentation by MHC class I molecules on DCs, whereas CTA may not be taken up to affect DCs. When DCs from GM1-lacking mice were matured in vitro, CT failed to up-regulate the expression of maturation markers and, thus, the binding of B subunits in CT to GM1 molecules on DCs is essential for the induction of DC maturation (37). It has been reported that CTA is required to not only assist in maturation but also to generate the migration of DCs (39, 40); therefore, CTB-mediated matured DCs can initiate their migration to secondary lymphoid organs and colocalization with naive T cells (38). Indeed, CT-loaded but not CTB-loaded DCs could migrate from marginal zones to T cell zones in the spleen (39) and from the subepithelial dome region to T cell zones in PPs (40); therefore, both CTA and CTB were essential for cross-priming CTLs in vivo and neither CTA nor CTB alone could induce CTLs at various compartments (Fig. 3). Taken together, although the detailed mechanisms of efficient Ag presentation via MHC class I and the maturation and migration of DCs by CT are still unknown, digested OVA might be efficiently captured by immature gut mucosal DCs in the presence of CTB and the captured Ag may be cross-presented by MHC class I during DC maturation and migration in the presence of CTA, resulting in the induction of mucosal class I MHC molecule-restricted CTLs that may cause the regression of previously established tumors.

OVA-specific $CD8^+$ CTLs were induced among not only the IELs but also the LPLs of the stomach, small intestine, and large intestine by oral administration of OVA plus CT, a higher percentage of OVA-specific CD8 CTLs was observed in the stomach, small intestine, and large intestine in order, and more specific CTLs were always detected among IELs than among LPLs (Fig. 4, *E* and *F*). Thus, CTLs are much easier to be induced in the upper and more superficial portions of the gastrointestinal tract when Ags are orally administrated with intact CT.

It has been reported that DCs in gastric mucosa are increased in *Helicobacter pylori* (*Hp*)-infected mice and that the response of DCs and T cells to *Hp* Ag is critical for *Hp*-induced gastritis (41). In the present study, Ag-specific CTLs in the stomach might be generated by mucosally activated DCs in the presence of CT and infiltrate-implanted gastric tumor tissues. It is possible that intestinally activated CTLs might migrate to the tumor-implanted stomach, which might also cause CTL infiltration. Actually, such effector CTLs usually express high levels of $\alpha_4\beta_7$ integrin and can home in to the gastric (42), and small and large intestinal mucosa (43) where mucosal addressin cell-adhesion molecule-1 (MadCAM-1), the ligand of $\alpha_4\beta_7$ integrin, is constitutively expressed by post-capillary endothelial cells in small (44, 45) and large intestinal lamina propria (46). Moreover, the number of gastric $\alpha_4\beta_7^{high}$ T cells increased markedly by oral administration of CT in mice (42). It has also been reported that MAdCAM-1 expression is increased in the gastric mucosa after oral administration with cholera vaccine composed of CTB and formalin-inactivated *V. cholerae* (47); therefore, MadCAM-1-expression in gastric mucosa and the recruitment of effector $\alpha4\beta7^{high}$ T cells to gastric mucosa might be enhanced by oral administration of the CT adjuvant and, thus, OVA-specific effector CTLs might efficiently infiltrate the OVA Ag-expressing tumor region in the stomach.

In the present study, we found that the growth of dermally implanted tumors was also suppressed by the oral administration of tumor Ag plus whole intact CT. The actual mechanisms for such suppression remains to be elucidated, but there are at least three distinct possibilities: first, the migration of Ag-specific CTLs from the gastrointestinal tract to the skin; second, the migration of Ag-presenting DCs activated in the mucosal compartments by CT; and third, the migration of both cells from the gastrointestinal tract to the skin at the same time. It has been reported that the levels of CCR4 expression, which is associated with T cell homing to the skin, are increased in gastric T cells by infection with *Hp* in humans (48). Moreover, mucosal DCs that take up Ag might migrate to regional lymph nodes near the dermal tumor and prime the CTLs there, and the CTLs could effectively infiltrate dermal tumor tissue. Indeed, Belyakov et al. demonstrated an opposite mechanism in which skin-derived DCs containing heat-labile enterotoxin of *Escherichia coli* migrated to PPs and induced mucosal CTLs by transcutaneous immunization of an Ag and CT (49). Although the detailed mechanisms of this migration of DCs between skin and mucosa are unknown, they have clearly shown that DCs can migrate between the mucosa and skin. We are currently comparing the alteration of DCs in the mucosal compartment, spleen, and lymph nodes after oral administration of an Ag plus natural CT.

Unfortunately, such natural CT is not an appropriate mucosal adjuvant for human clinical investigation (50); however, studies

using natural CT would provide important and critical information about the effect of CT that would be useful for mucosal immune activation. Based on the findings obtained by using natural CT in a mouse model system, we could establish much safer protocols with a mutant CT (51) that induces adenosine diphosphate ribosylation and cyclic adenosine monophosphate formation, which may prevent severe diarrhea as well as retain adjuvant properties. Taken together, an artificial CT-based vaccine targeting DCs may provide a strategy for efficient CTL induction and avirulent mucosal cancer vaccination.

Our data also indicate that E.G7-OVA tumor growth was suppressed by OVA-specific CTLs but not NK cells (Fig. 7*B*). Vaccination with OVA-CT-pulsed DC protects against E.G7-OVA tumor development in vivo in wild-type, NK-depleted, and CD4-deficient mice but not in CD8-deficient mice (34), indicating that the E.G7-OVA tumor might be controlled by CD8 T cells but not by NK cells or CD4 T cells. In fact, TILs in the suppressed tumor did not show any NK-related cytotoxicity (Fig. 7*B*). Moreover, it has been demonstrated that in vitro pretreatment of NK cells with CT inhibits NK cell killing of tumor (YAC-1 or P815), because G proteins in NK cell membranes are ADP ribosylated with CT and ribosylation inhibits the lysis of tumor cells (52); therefore, NK cells do not seem to be involved in the suppression of E.G7-OVA growth in vivo.

It has been shown that activated CTLs but not naive CTLs can represent antitumor (22) or antivirus (12) responses in vivo. In the present study, already established E.G7 tumor growth can be suppressed only when OVA-specific CTLs that show specific cytotoxicity without requiring in vitro restimulation are induced, particularly in the mucosal compartment. To our knowledge, this is the first demonstration of the visual suppression of already established tumor growth by the simple oral administration of tumor Ag plus mucosal adjuvant. The findings shown in the present study herald a new era for cancer immunotherapy.

Acknowledgments

We thank Dr. Yoshihiro Kumagai and Yoshihiko Norose for useful discussions and advice.

Disclosures

The authors have no financial conflict of interest.

References

1. Franks, L. M., and M. A. Knowles. 2005. What is cancer? In *Introduction to the Cellular and Molecular Biology of Cancer*, 4th Ed. M. A. Knowles and P. J. Selby, eds. Oxford University Press, New York, pp. 1–24.
2. Finn, O. J. 2003. Cancer vaccines: between the idea and the reality. *Nat. Rev. Immunol.* 3: 630–641.
3. Czerkinsky, C., F. Anjuere, J. R. McGhee, A. George-Chandy, J. Holmgren, M. P. Kieny, K. Fujiyashi, J. F. Mestecky, V. Pierrefite-Carle, C. Rask, and J. B. Sun. 1999. Mucosal immunity and tolerance: relevance to vaccine development. *Immunol. Rev.* 170: 197–222.
4. Yuki, Y., and H. Kiyono. 2003. New generation of mucosal adjuvants for the induction of protective immunity. *Rev. Med. Virol.* 13: 293–310.
5. Takahashi, H. 2003. Antigen presentation in vaccine development. *Comp. Immunol. Microbiol. Infect. Dis.* 26: 309–328.
6. Hayday, A., E. Theodoridis, E. Ramsburg, and J. Shires. 2001. Intraepithelial lymphocytes: exploring the third way in immunology. *Nat. Immunol.* 2: 997–1003.
7. Offit, P. A., and K. I. Dudzik. 1989. Rotavirus-specific cytotoxic T lymphocytes appear at the intestinal mucosal surface after rotavirus infection. *J. Virol.* 63: 3507–3512.
8. Chardes, T., D. Buzoni-Gatel, A. Lepage, F. Bernard, and D. Bout. 1994. *Toxoplasma gondii* oral infection induces specific cytotoxic CD8 $\alpha\beta^+$ Thy-1$^+$ gut intraepithelial lymphocytes, lytic for parasite-infected enterocytes. *J. Immunol.* 153: 4596–4603.
9. Muller, S., M. Buhler-Jungo, and C. Mueller. 2000. Intestinal intraepithelial lymphocytes exert potent protective cytotoxic activity during an acute virus infection. *J. Immunol.* 164: 1986–1994.
10. Taunk, J., A. I. Roberts, and E. C. Ebert. 1992. Spontaneous cytotoxicity of human intraepithelial lymphocytes against epithelial cell tumors. *Gastroenterology* 102: 69–75.
11. Roberts, A. I., S. M. O'Connell, L. Biancone, R. E. Brolin, and E. C. Ebert. 1993. Spontaneous cytotoxicity of intestinal intraepithelial lymphocytes: clues to the mechanism. *Clin. Exp. Immunol.* 94: 527–532.
12. Kuribayashi, H., A. Wakabayashi, M. Shimizu, H. Kaneko, Y. Norose, Y. Nakagawa, J. Wang, Y. Kumagai, D. H. Margulies, and H. Takahashi. 2004. Resistance to viral infection by intraepithelial lymphocytes in HIV-1 P18-I10-specific T-cell receptor transgenic mice. *Biochem. Biophys. Res. Commun.* 316: 356–363.
13. Takahashi, H., J. Cohen, A. Hosmalin, K. B. Cease, R. Houghten, J. L. Cornette, C. DeLisi, B. Moss, R. N. Germain, and J. A. Berzofsky. 1988. An immunodominant epitope of the human immunodeficiency virus envelope glycoprotein gp160 recognized by class I major histocompatibility complex molecule-restricted murine cytotoxic T lymphocytes. *Proc. Natl. Acad. Sci. USA* 85: 3105–3109.
14. Williams, N. A., T. R. Hirst, and T. O. Nashar. 1999. Immune modulation by the cholera-like enterotoxins: from adjuvant to therapeutic. *Immunol. Today* 20: 95–101.
15. Lencer, W. I., and B. Tsai. 2003. The intracellular voyage of cholera toxin: going retro. *Trends Biochem. Sci.* 28: 639–645.
16. Elson, C. O., and W. Ealding. 1984. Generalized systemic and mucosal immunity in mice after mucosal stimulation with cholera toxin. *J. Immunol.* 132: 2736–2741.
17. Marinaro, M., H. F. Staats, T. Hiroi, R. J. Jackson, M. Coste, P. N. Boyaka, N. Okahashi, M. Yamamoto, H. Kiyono, H. Bluethmann, et al. 1995. Mucosal adjuvant effect of cholera toxin in mice results from induction of T helper 2 (Th2) cells and IL-4. *J. Immunol.* 155: 4621–4629.
18. Bowen, J. C., S. K. Nair, R. Reddy, and B. T. Rouse. 1994. Cholera toxin acts as a potent adjuvant for the induction of cytotoxic T-lymphocyte responses with non-replicating antigens. *Immunology* 81: 338–342.
19. Carbone, F. R., and M. J. Bevan. 1989. Induction of ovalbumin-specific cytotoxic T cells by in vivo peptide immunization. *J. Exp. Med.* 169: 603–612.
20. Moore, M. W., F. R. Carbone, and M. J. Bevan. 1988. Introduction of soluble protein into the class I pathway of antigen processing and presentation. *Cell* 54: 777–785.
21. Porgador, A., H. F. Staats, B. Faiola, E. Gilboa, and T. J. Palker. 1997. Intranasal immunization with CTL epitope peptides from HIV-1 or ovalbumin and the mucosal adjuvant cholera toxin induces peptide-specific CTLs and protection against tumor development in vivo. *J. Immunol.* 158: 834–841.
22. Dalyot-Herman, N., O. F. Bathe, and T. R. Malek. 2000. Reversal of CD8$^+$ T cell ignorance and induction of anti-tumor immunity by peptide-pulsed APC. *J. Immunol.* 165: 6731–6737.
23. Eriksson, K., J. B. Sun, I. Nordstrom, M. Fredriksson, M. Lindblad, B. L. Li, and J. Holmgren. 2004. Coupling of antigen to cholera toxin for dendritic cell vaccination promotes the induction of MHC class I-restricted cytotoxic T cells and the rejection of a cognate antigen-expressing model tumor. *Eur. J. Immunol.* 34: 1272–1281.
24. Taguchi, T., J. R. McGhee, R. L. Coffman, K. W. Beagley, J. H. Eldridge, K. Takatsu, and H. Kiyono. 1990. Analysis of Th1 and Th2 cells in murine gut-associated tissues: frequencies of CD4$^+$ and CD8$^+$ T cells that secrete IFN-γ and IL-5. *J. Immunol.* 145: 68–77.
25. Takahashi, M., E. Osono, Y. Nakagawa, J. Wang, J. A. Berzofsky, D. H. Margulies, and H. Takahashi. 2002. Rapid induction of apoptosis in CD8$^+$ HIV-1 envelope-specific murine CTLs by short exposure to antigenic peptide. *J. Immunol.* 169: 6588–6593.
26. Semple, J. W., and M. R. Szewczuk. 1986. Natural killer cells in murine muscular dystrophy: IV. Characterization of Percoll fractionated splenic and thymic natural killer cells and natural killer-sensitive thymocyte targets. *Clin. Immunol. Immunopathol.* 41: 116–129.
27. Belz, G. T., W. Xie, and P. C. Doherty. 2001. Diversity of epitope and cytokine profiles for primary and secondary influenza a virus-specific CD8$^+$ T cell responses. *J. Immunol.* 166: 4627–4633.
28. Nakatsuka, K., H. Sugiyama, Y. Nakagawa, and H. Takahashi. 1999. Purification of antigenic peptide from murine hepatoma cells recognized by class-I major histocompatibility complex molecule-restricted cytotoxic T-lymphocytes induced with B7-1-gene-transfected hepatoma cells. *J. Hepatol.* 30: 1119–1129.
29. Kilshaw, P. J., and K. C. Baker. 1988. A unique surface antigen on intraepithelial lymphocytes in the mouse. *Immunol. Lett.* 18: 149–154.
30. Russell, G. J., C. M. Parker, K. L. Cepek, D. A. Mandelbrot, A. Sood, E. Mizoguchi, E. C. Ebert, M. B. Brenner, and A. K. Bhan. 1994. Distinct structural and functional epitopes of the α E β 7 integrin. *Eur. J. Immunol.* 24: 2832–2841.
31. Lefrancois, L., T. A. Barrett, W. L. Havran, and L. Puddington. 1994. Developmental expression of the α IEL β 7 integrin on T cell receptor γ δ and T cell receptor α β T cells. *Eur. J. Immunol.* 24: 635–640.
32. Rocha, B., P. Vassalli, and D. Guy-Grand. 1994. Thymic and extrathymic origins of gut intraepithelial lymphocyte populations in mice. *J. Exp. Med.* 180: 681–686.
33. Wakabayashi, A., Y. Kumagai, E. Watari, M. Shimizu, M. Utsuyama, K. Hirokawa, and H. Takahashi. 2006. Importance of gastrointestinal ingestion and macromolecular antigens in the vein for oral tolerance induction. *Immunology* 119: 167–177.
34. Sun, J. B., K. Eriksson, B. L. Li, M. Lindblad, J. Azem, and J. Holmgren. 2004. Vaccination with dendritic cells pulsed in vitro with tumor antigen conjugated to cholera toxin efficiently induces specific tumoricidal CD8$^+$ cytotoxic lymphocytes dependent on cyclic AMP activation of dendritic cells. *Clin. Immunol.* 112: 35–44.

35. Fujimoto, C., Y. Nakagawa, K. Ohara, and H. Takahashi. 2004. Polyriboinosinic polyribocytidylic acid [poly(I:C)]/TLR3 signaling allows class I processing of exogenous protein and induction of HIV-specific $CD8^+$ cytotoxic T lymphocytes. *Int. Immunol.* 16: 55–63.
36. Schulz, O., S. S. Diebold, M. Chen, T. I. Naslund, M. A. Nolte, L. Alexopoulou, Y. T. Azuma, R. A. Flavell, P. Liljestrom, and C. Reis e Sousa. 2005. Toll-like receptor 3 promotes cross-priming to virus-infected cells. *Nature* 433: 887–892.
37. Kawamura, Y. I., R. Kawashima, Y. Shirai, R. Kato, T. Hamabata, M. Yamamoto, K. Furukawa, K. Fujihashi, J. R. McGhee, H. Hayashi, and T. Dohi. 2003. Cholera toxin activates dendritic cells through dependence on GM1-ganglioside which is mediated by NF-κB translocation. *Eur. J. Immunol.* 33: 3205–3212.
38. Gagliardi, M. C., F. Sallusto, M. Marinaro, A. Langenkamp, A. Lanzavecchia, and M. T. De Magistris. 2000. Cholera toxin induces maturation of human dendritic cells and licences them for Th2 priming. *Eur. J. Immunol.* 30: 2394–2403.
39. Grdic, D., L. Ekman, K. Schon, K. Lindgren, J. Mattsson, K. E. Magnusson, P. Ricciardi-Castagnoli, and N. Lycke. 2005. Splenic marginal zone dendritic cells mediate the cholera toxin adjuvant effect: dependence on the ADP-ribosyltransferase activity of the holotoxin. *J. Immunol.* 175: 5192–5202.
40. Shreedhar, V. K., B. L. Kelsall, and M. R. Neutra. 2003. Cholera toxin induces migration of dendritic cells from the subepithelial dome region to T- and B-cell areas of Peyer's patches. *Infect. Immun.* 71: 504–509.
41. Drakes, M. L., S. J. Czinn, and T. G. Blanchard. 2006. Regulation of murine dendritic cell immune responses by *Helicobacter felis* antigen. *Infect. Immun.* 74: 4624–4633.
42. Michetti, M., C. P. Kelly, J. P. Kraehenbuhl, H. Bouzourene, and P. Michetti. 2000. Gastric mucosal $\alpha_4\beta_7$-integrin-positive CD4 T lymphocytes and immune protection against *Helicobacter* infection in mice. *Gastroenterology* 119: 109–118.
43. Lefrancois, L., C. M. Parker, S. Olson, W. Muller, N. Wagner, M. P. Schon, and L. Puddington. 1999. The role of β_7 integrins in CD8 T cell trafficking during an antiviral immune response. *J. Exp. Med.* 189: 1631–1638.
44. Berlin, C., R. F. Bargatze, J. J. Campbell, U. H. von Andrian, M. C. Szabo, S. R. Hasslen, R. D. Nelson, E. L. Berg, S. L. Erlandsen, and E. C. Butcher. 1995. α_4 integrins mediate lymphocyte attachment and rolling under physiologic flow. *Cell* 80: 413–422.
45. Berlin, C., E. L. Berg, M. J. Briskin, D. P. Andrew, P. J. Kilshaw, B. Holzmann, I. L. Weissman, A. Hamann, and E. C. Butcher. 1993. $\alpha_4\beta_7$ integrin mediates lymphocyte binding to the mucosal vascular addressin MAdCAM-1. *Cell* 74: 185–195.
46. Streeter, P. R., E. L. Berg, B. T. Rouse, R. F. Bargatze, and E. C. Butcher. 1988. A tissue-specific endothelial cell molecule involved in lymphocyte homing. *Nature* 331: 41–46.
47. Lindholm, C., A. Naylor, E. L. Johansson, and M. Quiding-Jarbrink. 2004. Mucosal vaccination increases endothelial expression of mucosal addressin cell adhesion molecule 1 in the human gastrointestinal tract. *Infect. Immun.* 72: 1004–1009.
48. Lundgren, A., C. Trollmo, A. Edebo, A. M. Svennerholm, and B. S. Lundin. 2005. *Helicobacter pylori*-specific $CD4^+$ T cells home to and accumulate in the human *Helicobacter pylori*-infected gastric mucosa. *Infect. Immun.* 73: 5612–5619.
49. Belyakov, I. M., S. A. Hammond, J. D. Ahlers, G. M. Glenn, and J. A. Berzofsky. 2004. Transcutaneous immunization induces mucosal CTLs and protective immunity by migration of primed skin dendritic cells. *J. Clin. Invest.* 113: 998–1007.
50. Clarke, L. L., B. R. Grubb, S. E. Gabriel, O. Smithies, B. H. Koller, and R. C. Boucher. 1992. Defective epithelial chloride transport in a gene-targeted mouse model of cystic fibrosis. *Science* 257: 1125–1128.
51. Yamamoto, S., Y. Takeda, M. Yamamoto, H. Kurazono, K. Imaoka, M. Yamamoto, K. Fujihashi, M. Noda, H. Kiyono, and J. R. McGhee. 1997. Mutants in the ADP-ribosyltransferase cleft of cholera toxin lack diarrheagenicity but retain adjuvanticity. *J. Exp. Med.* 185: 1203–1210.
52. Maghazachi, A. A., A. Al-Aoukaty, C. Naper, K. M. Torgersen, and B. Rolstad. 1996. Preferential involvement of Go and Gz proteins in mediating rat natural killer cell lysis of allogeneic and tumor target cells. *J. Immunol.* 157: 5308–5314.

JOURNAL OF VIROLOGY, June 2008, p. 6039–6044 Vol. 82, No. 12
0022-538X/08/$08.00+0 doi:10.1128/JVI.02753-07

Small Intestine CD4$^+$ T Cells Are Profoundly Depleted during Acute Simian-Human Immunodeficiency Virus Infection, Regardless of Viral Pathogenicity$^\nabla$

Yoshinori Fukazawa,[1]† Ariko Miyake,[1,2]† Kentaro Ibuki,[1] Katsuhisa Inaba,[1] Naoki Saito,[1] Makiko Motohara,[1] Reii Horiuchi,[1] Ai Himeno,[1] Kenta Matsuda,[1] Megumi Matsuyama,[1] Hidemi Takahashi,[3] Masanori Hayami,[1] Tatsuhiko Igarashi,[1] and Tomoyuki Miura[1]*

Laboratory of Primate Model, Experimental Research Center for Infectious Diseases, Institute for Virus Research, Kyoto University, 53 Shogoinkawaramachi, Sakyo-ku, Kyoto 606-8507, Japan[1]; *Laboratory of Tumor Cell Biology, Department of Medical Genome Sciences, Graduate School of Frontier Sciences, The University of Tokyo, Tokyo 162-8640, Japan*[2]; *and Department of Microbiology and Immunology, Nippon Medical School, Tokyo 113-8602, Japan*[3]

Received 27 December 2007/Accepted 27 March 2008

To analyze the relationship between acute virus-induced injury and the subsequent disease phenotype, we compared the virus replication and CD4$^+$ T-cell profiles for monkeys infected with isogenic highly pathogenic (KS661) and moderately pathogenic (#64) simian-human immunodeficiency viruses (SHIVs). Intrarectal infusion of SHIV-KS661 resulted in rapid, systemic, and massive virus replication, while SHIV-#64 replicated more slowly and reached lower titers. Whereas KS661 systemically depleted CD4$^+$ T cells, #64 caused significant CD4$^+$ T-cell depletion only in the small intestine. We conclude that SHIV, regardless of pathogenicity, can cause injury to the small intestine and leads to CD4$^+$ T-cell depletion in infected animals during acute infection.

The highly pathogenic simian-human immunodeficiency virus (SHIV) SHIV-C2/1-KS661 (KS661), which was derived from SHIV-89.6 (23), replicates to high titers and causes the irreversible depletion of the circulating CD4$^+$ T cells during the acute phase of intravenous infection, followed by AIDS-like disease within 1 year (23). We previously reported that KS661 massively replicates and depletes CD4$^+$ T cells in both peripheral and mucosal lymphoid tissues during the initial 4 weeks postinfection (16). On the other hand, the isogenic SHIV-#64 (#64), which was derived from SHIV-89.6P, is moderately pathogenic. The genomic sequences of the two SHIVs differ by only 0.16%, resulting in a total of six amino acid changes in the products of the *pol*, *env-gp41*, and *rev* genes. The intravenous inoculation of rhesus macaques with #64 induces plasma viral burdens comparable to those induced by KS661 during the acute phase of infection and causes a transient reduction of the circulating CD4$^+$ T lymphocytes (10). After the acute phase, the viral loads decline to undetectable levels and the populations of CD4$^+$ T cells recover to preinfection levels.

To clarify the relationship between acute viral replication kinetics and subsequent clinical courses for these isogenic SHIVs with distinct pathogenicities, we examined proviral DNA, infectious-virus-producing cells (IVPCs), and CD4$^+$ T-cell depletion in peripheral and mucosal lymphoid tissues of 17 infected (Table 1) and 7 uninfected adult rhesus macaques (*Macaca mulatta*). Both Chinese and Indian rhesus monkeys were randomly assigned to these groups. The monkeys were used in accordance with the institutional regulations approved by the Committee for Experimental Use of Nonhuman Primates of the Institute for Virus Research, Kyoto University, Kyoto, Japan. The animals were inoculated via intrarectal infusion as described previously (17). Following serial euthanasia, tissues were collected and analyzed up to 27 days postinfection (dpi) as described previously (16, 17).

Gross virus replication was assessed by measuring plasma viral loads by reverse transcriptase PCR (16). By 6 dpi, plasma viral RNA levels became detectable in all the KS661-infected macaques (Fig. 1A) and three of seven #64-infected macaques (animals MM372, MM391, and MM374) (Fig. 1B). Although the plasma viral loads of the two groups at 13 dpi, when the virus loads reached their initial peaks, were not significantly different ($P = 0.1673$), the average load (± the standard deviation) in KS661-infected monkeys ($9.3 \times 10^8 \pm 15.9 \times 10^8$ copies/ml) was about 10 times higher than that in #64-infected monkeys ($6.3 \times 10^7 \pm 11.6 \times 10^7$ copies/ml). These results suggest that KS661 spread faster and reached a somewhat higher titer than did #64 when the viruses were inoculated intrarectally.

Levels of peripheral blood CD4$^+$ T lymphocytes in all the KS661-infected monkeys decreased substantially within 4 weeks (Fig. 1C). On the other hand, the reductions in the levels of CD4$^+$ T cells varied among the #64-infected monkeys (Fig. 1D). For example, MM378 did not exhibit any appreciable changes, even though the plasma viral RNA load in this monkey reached 2.6×10^7 copies/ml by 21 dpi (Fig. 1 B and D).

* Corresponding author. Mailing address: Laboratory of Primate Model, Experimental Research Center for Infectious Diseases, Institute for Virus Research, Kyoto University, 53 Shogoinkawaramachi, Sakyo-ku, Kyoto 606-8507, Japan. Phone: 81-75-751-3984. Fax: 81-75-761-9335. E-mail: tmiura@virus.kyoto-u.ac.jp.
† These authors contributed equally to this work.
▽ Published ahead of print on 9 April 2007.

TABLE 1. Experimental schedule for individual monkeys[a]

Virus (inoculum size)	Monkeys examined at:		
	6 dpi	13 dpi	27 dpi
KS661 (2×10^5 $TCID_{50}$)	MM300, MM309	MM313, MM334, MM392, MM393	MM308, MM310, MM394, MM395
#64 (2×10^5 $TCID_{50}$)	MM379, MM390	MM372, MM373[b], MM391	MM374, MM378

[a] $TCID_{50}$, 50% tissue culture infective doses; [b], MM373 received 2×10^3 $TCID_{50}$ of #64.

These data suggest that the decline in circulating $CD4^+$ T cells in KS661-infected animals was more severe and more reproducible than that in the #64-infected monkeys.

Another highly pathogenic SHIV, SHIV-DH12R, is known to cause systemic and synchronous replication events in animals following intravenous inoculation (6). To reveal the spread of virus in monkeys following intrarectal infection, we measured proviral DNA loads in a variety of tissues as described previously (16). KS661 proviral DNA was detected not only in samples from the rectums, the site of virus inoculation, but also in peripheral blood mononuclear cells and some lymph nodes (LN) at 6 dpi (Fig. 2A), suggesting that the virus was already spreading systemically. At 13 dpi, when the viral RNA loads in peripheral blood increased to the highest titers, proviral DNA levels in all of the tissues examined also increased, with levels in most monkeys exceeding 10^4 copies/μg of DNA. The levels of proviral DNA in all the tissues declined remarkably by 27 dpi. In contrast, #64 proviral DNA was detected only in the rectum of one (MM390) of the two monkeys examined at 6 dpi (Fig. 2A). At 13 dpi, the amount of proviral DNA in each tissue sample from #64-infected monkeys ($<10^4$ copies/μg of DNA) was considerably smaller than

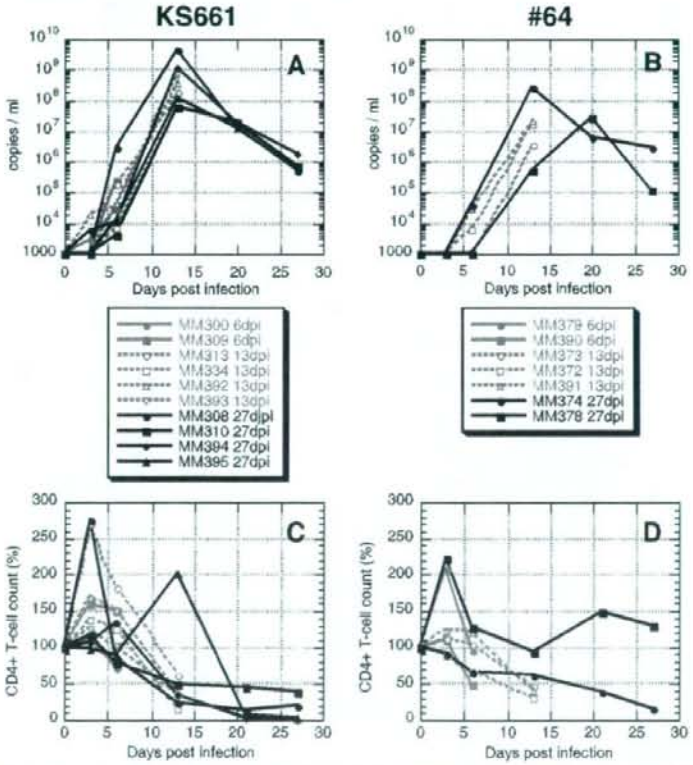

FIG. 1. Plasma viral RNA loads and profiles of circulating $CD4^+$ T cells for monkeys intrarectally infected with highly pathogenic KS661 and moderately pathogenic #64. (A and B) Plasma viral RNA loads were measured by quantitative reverse transcriptase PCR. The detection limit of this assay was 10^3 copies/ml. (C and D) Levels of $CD4^+$ T cells in peripheral blood samples from monkeys infected with KS661 and #64. The absolute number of $CD3^+$ $CD4^+$ cells in peripheral blood immediately before infection (day 0 postinfection) was defined as 100% for each monkey.

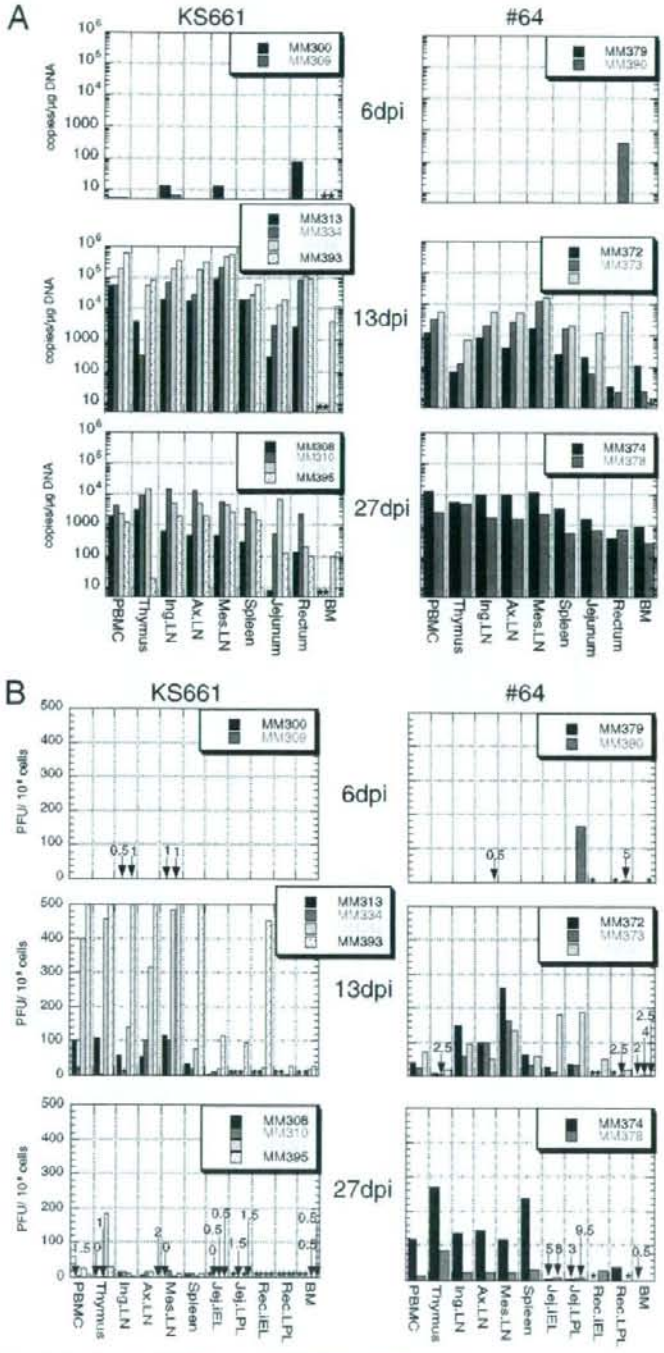

FIG. 2. (A) Proviral DNA loads in tissues of KS661- and #64-infected monkeys at 6, 13, and 27 dpi. Viral burdens were determined by quantitative PCR and expressed as the numbers of viral DNA copies per microgram of total DNA extracted from tissue homogenates. PBMC, peripheral blood mononuclear cells; Ing., inguinal; Ax., axillary; Mes., mesenteric; BM, bone marrow; *, not done. (B) Numbers of IVPCs in tissues of KS661- and #64-infected monkeys at 6, 13, and 27 dpi. Numbers of IVPCs were determined by an infectious plaque assay and were expressed as the numbers of PFU per 10^6 cells. Jej., jejunum; Rec., rectum; iEL, intraepithelial lymphocytes; *, not done.

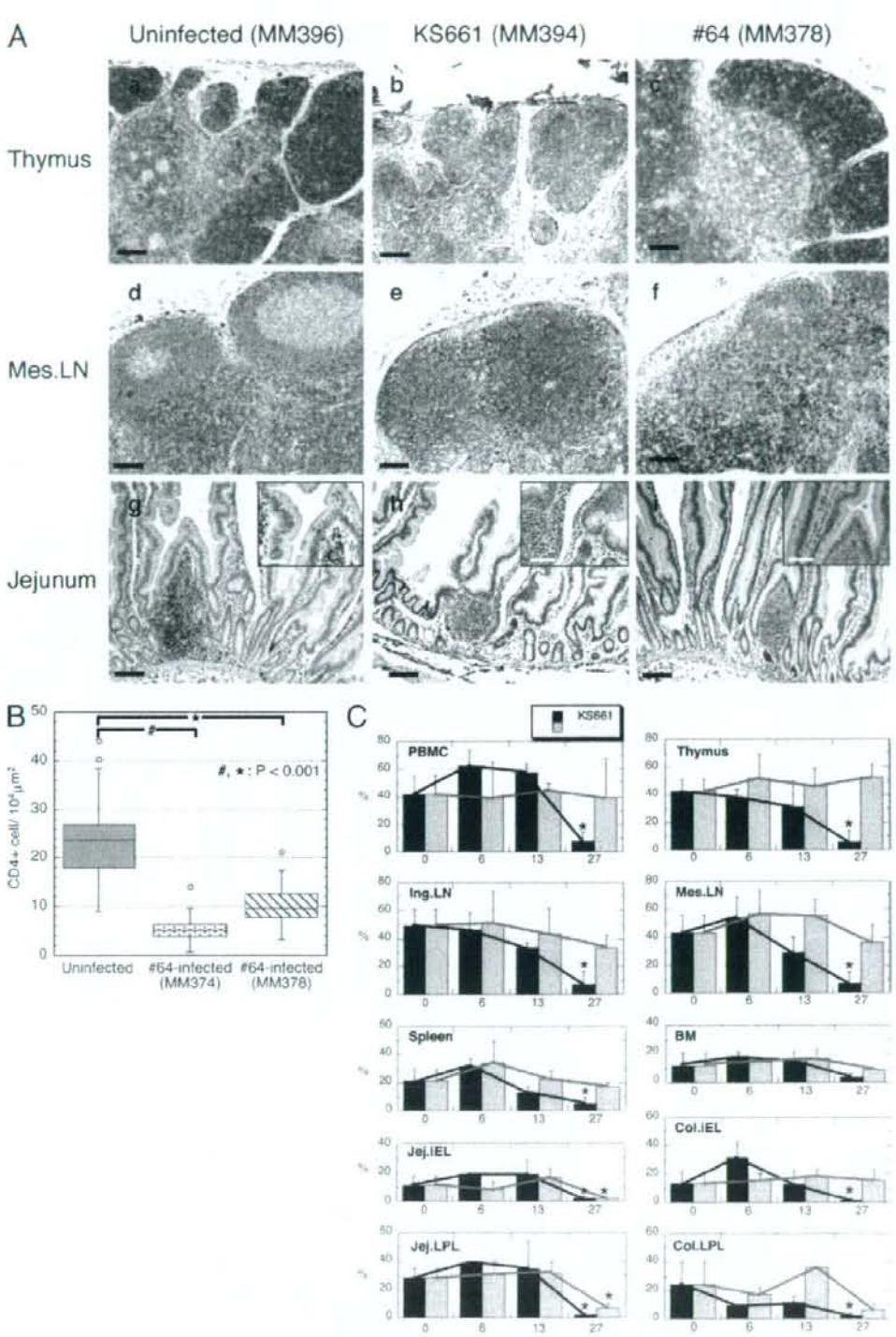

that in each sample from the KS661-infected monkeys. However, unlike the KS661 proviral DNA levels, the #64 proviral DNA levels in most tissues were maintained up to 27 dpi. These results suggest that #64 spread more slowly than KS661 and that the amounts of proviral DNA in a variety of tissues from the #64-infected animals were smaller than those in the tissues from KS661-infected animals around the initial peak of plasma viremia.

Because the amount of proviral DNA measured by PCR may include nonreplicating remnants of the viral genome, we also measured the number of IVPCs in each tissue sample by a plaque assay as described previously (9, 15). Briefly, cells prepared from infected animals were mixed with human T-lymphoid M8166 indicator cells, resuspended in culture medium containing 0.4% agarose, and plated into petri dishes. The plaques that formed in the cell layer were counted after 10 days of cultivation, and the number of IVPCs was calculated. For the KS661-infected monkeys, high numbers of IVPCs in all the tissue samples examined at 13 dpi were detected (Fig. 2B). Among these samples, the thymus and mesenteric LN samples harbored especially high numbers of IVPCs (more than 500/10^6 cells) at 13 dpi. The numbers of IVPCs declined remarkably from 13 to 27 dpi. We concluded that KS661 replicated systemically and synchronously in a variety of tissues, including the intestinal tract, at 13 dpi. In contrast, #64 production patterns in different tissues were not synchronous. Among #64-infected monkeys at 6 dpi, virus production was most active in the jejunum lamina propria lymphocytes (LPL) of MM390 (166 IVPCs/10^6 cells). At 13 dpi, interestingly, mesenteric LN became the center of virus production in two of the three monkeys examined (MM372 and MM373; 259 and 160 IVPCs/10^6 cells). In the other monkey (MM391), the jejunum had the highest number of IVPCs, followed by the mesenteric LN. These results suggested that the virus that replicated in the jejunum spread directly into the mesenteric LN via the flow of lymphatic fluid. At 27 dpi, the thymus tissues of both monkeys examined (MM374 and MM378) exhibited the highest numbers of IVPCs. In summary, the systemic dissemination of #64 was slower than that of KS661, and it was particularly delayed in the thymus during the acute phase.

Systemic $CD4^+$ cell depletion is the signature of disease induced by highly pathogenic SHIVs (7, 8, 22). We therefore compared the frequencies of $CD4^+$ cells in tissues from the animals infected with KS661 and #64, in addition to those of the circulating $CD4^+$ T lymphocytes. As representatives of the major virus-producing organs, the thymus, the mesenteric LN, and the jejunum were selected for examination. CD4 cell numbers were measured by immunohistochemistry analyses as described previously (18). Uninfected thymus tissue contained abundant $CD4^+$ cells that were stained brown (Fig. 3A, panel a), while the tissue collected from the KS661-infected animal at 27 dpi harbored few such cells (Fig. 3A, panel b). #64 caused virtually no $CD4^+$ cell depletion in the thymus at 27 dpi (Fig. 3A, panel c). In the mesenteric LN of uninfected monkeys, $CD4^+$ cells were found in the paracortical region (Fig. 3A, panel d). KS661 depleted $CD4^+$ cells in this area (Fig. 3A, panel e). Unlike KS661, #64 did not reduce the level of $CD4^+$ cells (Fig. 3A, panel f). The jejunum samples from uninfected animals contained $CD4^+$ cells in the lamina propria and follicles of gut-associated lymphatic tissues (Fig. 3 A, panel g). KS661 depleted $CD4^+$ cells in these tissues, too (Fig. 3A, panel h). Interestingly, #64 caused $CD4^+$ cell depletion in the small intestine comparable to that caused by KS661 (Fig. 3A, panel i). To confirm the observed cell reduction in the jejunum samples, we randomly selected a total of 40 fields on the tissue sections from each animal for viewing at a total magnification of ×400, counted $CD4^+$ cells, and averaged the numbers (Fig. 3B). The $CD4^+$ cell densities in the jejunum samples from the #64-infected monkeys were significantly lower than those in the samples from uninfected animals ($P < 0.001$). This gut-specific $CD4^+$ cell depletion caused by #64 prompted us to analyze the frequencies of $CD4^+$ T cells (including CD4 and CD8 doubly positive cells) in a variety of tissues by flow cytometry (Fig. 3C). KS661 caused systemic $CD4^+$ T-lymphocyte depletion by 27 dpi (Fig. 3C). In agreement with the immunohistochemistry results, #64 significantly depleted $CD4^+$ T cells only in the jejunum intraepithelial lymphocytes and LPL ($P = 0.01$ and 0.003, respectively) (Fig. 3C) by 27 dpi, although we examined only two #64-infected monkeys at 27 dpi. In conclusion, the $CD4^+$ T-cell depletion patterns caused by KS661 and #64 were distinct, and the small intestine was the only site in which $CD4^+$ T cells were significantly depleted by the moderately pathogenic #64.

Taken together, our results show that #64 disseminated more slowly and replicated less than KS661 in systemic lymphoid tissues, as well as in peripheral blood, during the acute phase of infection. We believe that because of its low rate and low levels of replication, #64 could not cause irreversible injury before the host mounted an immune reaction. As a result, $CD4^+$ T cells were not completely depleted in all the tissues examined, except in the small intestine. These results suggest that the small intestine is the tissue most sensitive to virus-induced $CD4^+$ T-cell depletion during the acute phase of infection. Recent reports revealed that severe acute depletions

FIG. 3. Profiles of $CD4^+$ T cells in systemic lymphoid tissues during acute infection. (A) Immunohistochemical staining for CD4 molecules (stained brown) in the thymus, mesenteric (mes.) LN, and jejunum tissues of KS661- or #64-infected monkeys at 27 dpi, in addition to those of uninfected monkeys. Black scale bars, 100 μm; white scale bars in insets of panels g, h, and i, 50 μm. (B) Comparison of $CD4^+$ cell frequencies in the jejunum LPL of uninfected and #64-infected monkeys at 27 dpi. A total of forty randomly selected fields (total magnification, ×400) of at least four tissue sections per animal were used for the analysis of jejunum LPL. *P* values (determined by Student's *t* test with 95% confidence intervals) are for comparisons of each #64-infected monkey with uninfected monkeys. (C) Percentages of $CD4^+$ T cells among total lymphocytes from KS661- and #64-infected monkeys. In each graph, data for 0 dpi (time points postinfection are shown along the *x* axis) are averages of percentages for seven uninfected control monkeys. Percentages of $CD4^+$ T cells (including CD4 and CD8 doubly positive cells) were obtained by first gating lymphocytes and then $CD3^+$ T cells with a flow cytometer. PBMC, peripheral blood mononuclear cells; Ing., inguinal; Jej., jejunum; iEL, intraepithelial lymphocytes; BM, bone marrow; Col., colon; *, $P < 0.05$ (percentage at 0 dpi versus that at 27 dpi; Student's *t* test with a 95% confidence interval).

of mucosal CD4$^+$ T cells have been observed in simian immunodeficiency virus-infected monkeys (11, 12, 24, 25) and human immunodeficiency virus-infected humans (2, 5, 13). The acute depletion of mucosal CD4$^+$ T cells and the disease outcome are correlated (1, 3, 21, 26). However, a decrease of mucosal CD4$^+$ T cells has also been observed in the early phases of natural host infections, such as SIVagm infection in African green monkeys and SIVsmm infection in sooty mangabeys, which typically do not progress to AIDS (4, 14, 19). In addition, the levels of apoptosis and immune activation and the degrees of CD4$^+$ T-cell restoration differ between progressors and nonprogressors in simian immunodeficiency virus models (4, 14, 19). Taken together, these results raise the possibility that the severe acute depletion of mucosal CD4$^+$ T cells is not sufficient to induce AIDS. The restoration of CD4$^+$ T cells and normal immune function after the severe acute depletion may define the eventual disease outcome (20). The abilities of KS661- and #64-infected monkeys to restore the immune system may be different, because KS661, but not #64, impairs thymic T-cell differentiation (18). Currently, we are focusing on the restoration of CD4$^+$ T cells and the functional aspect of the immune cells in the small intestines of animals infected with KS661 and #64 to further clarify the determinant(s) of the disease outcome.

We are grateful to James Raymond for English editing of the manuscript and to Takahito Kazama for technical support.

This work was supported, in part, by Research on Human Immunodeficiency Virus/AIDS in Health and Labor Sciences research grants from the Ministry of Health, Labor and Welfare, Japan, a grant-in-aid for scientific research from the Ministry of Education and Science, Japan, a research grant for health sciences focusing on drug innovation for AIDS from the Japan Health Sciences Foundation, and a grant from the Program for the Promotion of Fundamental Studies in Health Sciences of the National Institute of Biomedical Innovation (NIBIO) of Japan.

REFERENCES

1. **Brenchley, J. M., D. A. Price, and D. C. Douek.** 2006. HIV disease: fallout from a mucosal catastrophe? Nat. Immunol. **7**:235–239.
2. **Brenchley, J. M., T. W. Schacker, L. E. Ruff, D. A. Price, J. H. Taylor, G. J. Beilman, P. L. Nguyen, A. Khoruts, M. Larson, A. T. Haase, and D. C. Douek.** 2004. CD4$^+$ T cell depletion during all stages of HIV disease occurs predominantly in the gastrointestinal tract. J. Exp. Med. **200**:749–759.
3. **Chase, A., Y. Zhou, and R. F. Siliciano.** 2006. HIV-1-induced depletion of CD4$^+$ T cells in the gut: mechanism and therapeutic implications. Trends Pharmacol. Sci. **27**:4–7.
4. **Gordon, S. N., N. R. Klatt, S. E. Bosinger, J. M. Brenchley, J. M. Milush, J. C. Engram, R. M. Dunham, M. Paiardini, S. Klucking, A. Danesh, E. A. Strobert, C. Apetrei, I. V. Pandrea, D. Kelvin, D. C. Douek, S. I. Staprans, D. L. Sodora, and G. Silvestri.** 2007. Severe depletion of mucosal CD4$^+$ T cells in AIDS-free simian immunodeficiency virus-infected sooty mangabeys. J. Immunol. **179**:3026–3034.
5. **Guadalupe, M., E. Reay, S. Sankaran, T. Prindiville, J. Flamm, A. McNeil, and S. Dandekar.** 2003. Severe CD4$^+$ T-cell depletion in gut lymphoid tissue during primary human immunodeficiency virus type 1 infection and substantial delay in restoration following highly active antiretroviral therapy. J. Virol. **77**:11708–11717.
6. **Igarashi, T., C. R. Brown, R. A. Byrum, Y. Nishimura, Y. Endo, R. J. Plishka, C. Buckler, A. Buckler-White, G. Miller, V. M. Hirsch, and M. A. Martin.** 2002. Rapid and irreversible CD4$^+$ T-cell depletion induced by the highly pathogenic simian/human immunodeficiency virus SHIV(DH12R) is systemic and synchronous. J. Virol. **76**:379–391.
7. **Igarashi, T., Y. Endo, G. Englund, R. Sadjadpour, T. Matano, C. Buckler, A. Buckler-White, R. Plishka, T. Theodore, R. Shibata, and M. A. Martin.** 1999. Emergence of a highly pathogenic simian/human immunodeficiency virus in a rhesus macaque treated with anti-CD8 mAb during a primary infection with a nonpathogenic virus. Proc. Natl. Acad. Sci. USA **96**:14049–14054.
8. **Joag, S. V., Z. Li, L. Foresman, E. B. Stephens, L.-J. Zhao, I. Adany, D. M. Pinson, H. M. McClure, and O. Narayan.** 1996. Chimeric simian/human immunodeficiency virus that causes progressive loss of CD4$^+$ T cells and AIDS in pig-tailed macaques. J. Virol. **70**:3189–3197.
9. **Kato, S., Y. Hiraishi, N. Nishimura, T. Sugita, M. Tomihama, and T. Takano.** 1998. A plaque hybridization assay for quantifying and cloning infectious human immunodeficiency virus type 1 virions. J. Virol. Methods **72**:1–7.
10. **Kozyrev, I. L., K. Ibuki, T. Shimada, T. Kuwata, T. Takemura, M. Hayami, and T. Miura.** 2001. Characterization of less pathogenic infectious molecular clones derived from acute-pathogenic SHIV-89.6p stock virus. Virology **282**:6–13.
11. **Li, Q., L. Duan, J. D. Estes, Z. M. Ma, T. Rourke, Y. Wang, C. Reilly, J. Carlis, C. J. Miller, and A. T. Haase.** 2005. Peak SIV replication in resting memory CD4$^+$ T cells depletes gut lamina propria CD4$^+$ T cells. Nature **434**:1148–1152.
12. **Mattapallil, J. J., D. C. Douek, B. Hill, Y. Nishimura, M. Martin, and M. Roederer.** 2005. Massive infection and loss of memory CD4$^+$ T cells in multiple tissues during acute SIV infection. Nature **434**:1093–1097.
13. **Mehandru, S., M. A. Poles, K. Tenner-Racz, A. Horowitz, A. Hurley, C. Hogan, D. Boden, P. Racz, and M. Markowitz.** 2004. Primary HIV-1 infection is associated with preferential depletion of CD4$^+$ T lymphocytes from effector sites in the gastrointestinal tract. J. Exp. Med. **200**:761–770.
14. **Milush, J. M., J. D. Reeves, S. N. Gordon, D. Zhou, A. Muthukumar, D. A. Kosub, E. Chacko, L. D. Giavedoni, C. C. Ibegbu, K. S. Cole, J. L. Miamidian, M. Paiardini, A. P. Barry, S. I. Staprans, G. Silvestri, and D. L. Sodora.** 2007. Virally induced CD4$^+$ T cell depletion is not sufficient to induce AIDS in a natural host. J. Immunol. **179**:3047–3056.
15. **Miyake, A., Y. Enose, S. Ohkura, H. Suzuki, T. Kuwata, T. Shimada, S. Kato, O. Narayan, and M. Hayami.** 2004. The quantity and diversity of infectious viruses in various tissues of SHIV-infected monkeys at the early and AIDS stages. Arch. Virol. **149**:943–955.
16. **Miyake, A., K. Ibuki, Y. Enose, H. Suzuki, R. Horiuchi, M. Motohara, N. Saito, T. Nakasone, M. Honda, T. Watanabe, T. Miura, and M. Hayami.** 2006. Rapid dissemination of a pathogenic simian/human immunodeficiency virus to systemic organs and active replication in lymphoid tissues following intrarectal infection. J. Gen. Virol. **87**:1311–1320.
17. **Miyake, A., K. Ibuki, H. Suzuki, R. Horiuchi, N. Saito, M. Motohara, M. Hayami, and T. Miura.** 2005. Early virological events in various tissues of newborn monkeys after intrarectal infection with pathogenic simian human immunodeficiency virus. J. Med. Primatol. **34**:294–302.
18. **Motohara, M., K. Ibuki, A. Miyake, Y. Fukazawa, K. Inaba, H. Suzuki, K. Masuda, N. Minato, H. Kawamoto, T. Nakasone, M. Honda, M. Hayami, and T. Miura.** 2006. Impaired T-cell differentiation in the thymus at the early stages of acute pathogenic chimeric simian-human immunodeficiency virus (SHIV) infection in contrast to less pathogenic SHIV infection. Microbes Infect. **8**:1539–1549.
19. **Pandrea, I. V., R. Gautam, R. M. Ribeiro, J. M. Brenchley, I. F. Butler, M. Pattison, T. Rasmussen, P. A. Marx, G. Silvestri, A. A. Lackner, A. S. Perelson, D. C. Douek, R. S. Veazey, and C. Apetrei.** 2007. Acute loss of intestinal CD4$^+$ T cells is not predictive of simian immunodeficiency virus virulence. J. Immunol. **179**:3035–3046.
20. **Picker, L. J.** 2006. Immunopathogenesis of AIDS virus infection. Curr. Opin. Immunol. **18**:399–405.
21. **Picker, L. J., and D. I. Watkins.** 2005. HIV pathogenesis: the first cut is the deepest. Nat. Immunol. **6**:430–432.
22. **Reimann, K. A., J. T. Li, R. Veazey, M. Halloran, I. W. Park, G. B. Karlsson, J. Sodroski, and N. L. Letvin.** 1996. A chimeric simian/human immunodeficiency virus expressing a primary patient human immunodeficiency virus type 1 isolate *env* causes an AIDS-like disease after in vivo passage in rhesus monkeys. J. Virol. **70**:6922–6928.
23. **Shinohara, K., K. Sakai, S. Ando, Y. Ami, N. Yoshino, E. Takahashi, K. Someya, Y. Suzaki, T. Nakasone, Y. Sasaki, M. Kaizu, Y. Lu, and M. Honda.** 1999. A highly pathogenic simian/human immunodeficiency virus with genetic changes in cynomolgus monkey. J. Gen. Virol. **80**:1231–1240.
24. **Smit-McBride, Z., J. J. Mattapallil, M. McChesney, D. Ferrick, and S. Dandekar.** 1998. Gastrointestinal T lymphocytes retain high potential for cytokine responses but have severe CD4$^+$ T-cell depletion at all stages of simian immunodeficiency virus infection compared to peripheral lymphocytes. J. Virol. **72**:6646–6656.
25. **Veazey, R. S., M. DeMaria, L. V. Chalifoux, D. E. Shvetz, D. R. Pauley, H. L. Knight, M. Rosenzweig, R. P. Johnson, R. C. Desrosiers, and A. A. Lackner.** 1998. Gastrointestinal tract as a major site of CD4$^+$ T cell depletion and viral replication in SIV infection. Science **280**:427–431.
26. **Veazey, R. S., and A. A. Lackner.** 2004. Getting to the guts of HIV pathogenesis. J. Exp. Med. **200**:697–700.

Flexible Cyclic Ethers/Polyethers as Novel P2-Ligands for HIV-1 Protease Inhibitors: Design, Synthesis, Biological Evaluation, and Protein−Ligand X-ray Studies†

Arun K. Ghosh,*,‡ Sandra Gemma,‡ Abigail Baldridge,‡ Yuan-Fang Wang,§ Andrey Yu. Kovalevsky,§ Yashiro Koh,∥ Irene T. Weber,§ and Hiroaki Mitsuya⊥,#

Departments of Chemistry and Medicinal Chemistry, Purdue University, 560 Oval Drive, West Lafayette, Indiana 47907, Department of Biology, Molecular Basis of Disease, Georgia State University, Atlanta, Georgia 30303, Kumamoto University School of Medicine, Kumamoto 860-8556, Japan, Department of Hematology and Infectious Diseases, Experimental Retrovirology Section, HIV and AIDS Malignancy Branch, National Cancer Institute, Bethesda, Maryland 20892

Received April 21, 2008

We report the design, synthesis, and biological evaluation of a series of novel HIV-1 protease inhibitors. The inhibitors incorporate stereochemically defined flexible cyclic ethers/polyethers as high affinity P2-ligands. Inhibitors containing small ring 1,3-dioxacycloalkanes have shown potent enzyme inhibitory and antiviral activity. Inhibitors **3d** and **3h** are the most active inhibitors. Inhibitor **3d** maintains excellent potency against a variety of multi-PI-resistant clinical strains. Our structure−activity studies indicate that the ring size, stereochemistry, and position of oxygens are important for the observed activity. Optically active synthesis of 1,3-dioxepan-5-ol along with the syntheses of various cyclic ether and polyether ligands have been described. A protein−ligand X-ray crystal structure of **3d**-bound HIV-1 protease was determined. The structure revealed that the P2-ligand makes extensive interactions including hydrogen bonding with the protease backbone in the S2-site. In addition, the P2-ligand in **3d** forms a unique water-mediated interaction with the NH of Gly-48.

Introduction

The introduction of protease inhibitors (PIs) into highly active antiretroviral therapy (HAART), a combination therapy based on coadministration of PIs with reverse-transcriptase inhibitors, marked the beginning of a new era in HIV/AIDS chemotherapy. HAART treatment regimens have led to a significant decline in the number of deaths due to HIV infection in the developed world.[1] Unfortunately, there are a number of factors that severely limit current HAART treatment regimens. High frequency of dosing, heavy pill burden, and issues of tolerability and toxicity can lead to poor adherence to treatment.[2] The need for more potent, less toxic drug regimens is quite apparent.

It is the rapid emergence of drug resistance, however, that is proving to be the most formidable problem. Mutations causing drug resistance are thought to occur spontaneously, through the recombination of mixed viral populations, and also due to drug pressure, particularly when administered at substandard doses.[3−6] A growing number of patients are developing multidrug-resistant HIV-1 variants.[7,8] There is ample evidence that these viral strains can be transmitted. Thus, the development of antiretroviral agents able to maintain potency against resistant HIV strains has become an urgent priority.

Darunavir (TMC-114, **1**, Figure 1) is a new nonpeptidic PI recently approved by the FDA for the treatment of antiretroviral therapy-experienced patients.[9] Inhibitor **1**, and its related analogue **2**, are exceedingly active against both wild-type and multidrug resistant HIV strains. Both PIs demonstrated potent

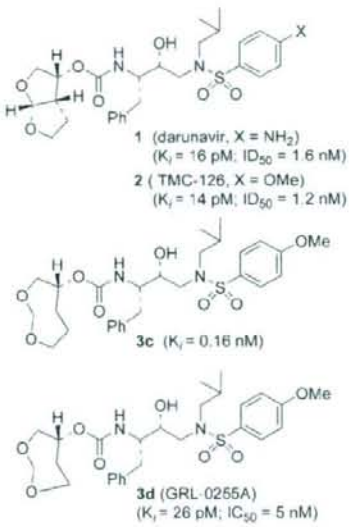

Figure 1. Structure of inhibitors **1**, **2**, and **3c**,**d**.

in vitro activity against viral isolates resistant to currently licensed PIs.[10−12] Our structure-based design strategies for these PIs are based on the presumption that maximizing active site interactions with the inhibitor, particularly hydrogen bonding with the protein backbone, would give rise to potent inhibitors retaining activity against mutant strains.[13,14] Indeed, side chain amino acid mutations cannot easily disrupt inhibitor−backbone interactions because the active site backbone conformation of mutant proteases is only minimally distorted compared to the wild-type HIV-1 protease.[15−17] In this context, the fused bis-tetrahydrofuran (bis-THF) urethane of compounds **1** and **2** was demonstrated to be a privileged P2-ligand, being able to engage

† The PDB accession code for **3d**-bound HIV-1 protease X-ray structure is 3DJK.

* To whom correspondence should be addressed. Phone: (765)-494-5323. Fax: (765)-496-1612. E-mail: akghosh@purdue.edu.

‡ Departments of Chemistry and Medicinal Chemistry, Purdue University.

§ Department of Biology, Molecular Basis of Disease, Georgia State University.

∥ Kumamoto University School of Medicine.

⊥ HIV and AIDS Malignancy Branch, National Cancer Institute.

10.1021/jm8004543 CCC: $40.75
Published on Web 09/11/2008

Table 1. Enzyme Inhibitory and Antiviral Activity of Inhibitors **3a**−**m**

entry	inhibitor	K_i (nM)	IC_{50} (nM)[a]	entry	inhibitor	K_i (nM)	IC_{50} (nM)[a]
1	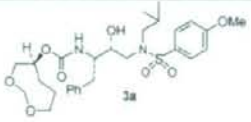 **3a**	0.15 ± 0.019	nd[b]	8	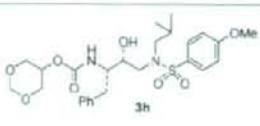 **3h**	0.041 ± 0.002	3.4 ± 0.7
2	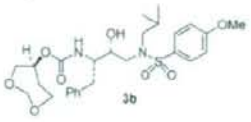 **3b**	0.16 ± 0.04	30 ± 1	9	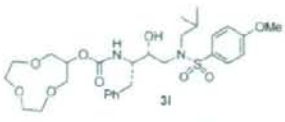 **3i**	16 ± 2.2	nd
3	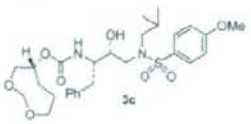 **3c**	0.16 ± 0.011	nd	10	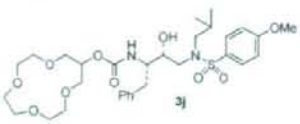 **3j**	33 ± 1.9	nd
4	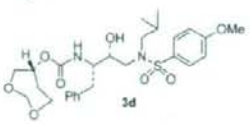 **3d**	0.026 ± 0.012	4.9 ± 0.3	11	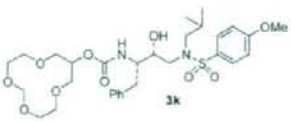 **3k**	6.3 ± 0.57	>1000
5	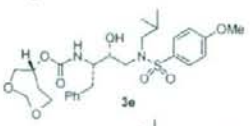 **3e**	0.81 ± 0.12	nd	12	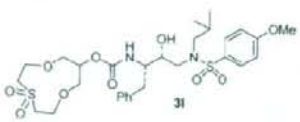 **3l**	1.9 ± 0.2	>1000
6	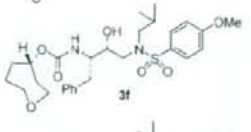 **3f**	0.74 ± 0.15	nd	13	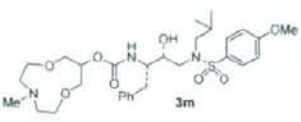 **3m**	19 ± 0.76	>1000
7	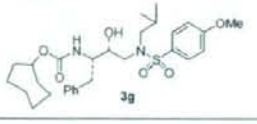 **3g**	27 ± 0.81	nd	SQV[c]	-	-	16 ± 3
				APV[d]	-	-	27 ± 6

[a] MT-2 human T-lymphoid cells exposed to HIV-1_{LAI}. [b] nd = not determined. [c] SQV = saquinavir. [d] APV = amprenavir.

in a number of hydrogen bonding interactions with the backbone atoms of amino acids at the protease S2-site.

We are continuing our efforts toward the development of novel PIs characterized by a high activity against both wild-type HIV-1 and resistant strains. We further speculated that an inhibitor interacting strongly with the protein backbone, while being able to accommodate amino acid side chain variations by means of repacking with a flexible ring, would maintain significant affinity against both wild-type and mutant enzymes. With this goal in mind, we designed a series of PIs based on the (*R*)-(hydroxyethylamino)sulfonamide isostere and bearing flexible cyclic ethers and polyethers as P2-ligands (inhibitors **3a**−**m**, Table 1). Starting from compound **3c**, incorporating a (1*R*)-3,5-dioxacyclooctan-1-yl urethane, which can be considered as the flexible counterpart of the bis-THF moiety, we designed a series of structural variants of this inhibitor. These inhibitors contain polyether-based P2-ligands ranging from 6- to 13-membered rings coupled to a *p*-methoxyphenylsulfonamide as the P2′-ligand. Herein we report the structure-based design, synthesis, and preliminary biological evaluation of inhibitors **3a**−**m**. Among these inhibitors, **3d** (Figure 1) is the most potent, with an impressive enzyme inhibitory and antiviral activity (K_i = 26 pM, IC_{50} = 4.9 nM). Furthermore, a protein−ligand X-ray structure of **3d**-bound HIV-1 protease has revealed important molecular insight regarding ligand-binding site interactions.

Chemistry. The syntheses of seven- and eight-membered 1,3-dioxacycloalkanes **8a**−**d** for the corresponding inhibitors **3a**−**d** are shown in Scheme 1. Protected diol **6a** was prepared by a two-step procedure starting from (*S*)-hydroxyglutaric acid **4**, obtained by following a known protocol.[18] The hydroxyl group of **4** was protected as a *tert*-butyldiphenylsilylether **5** in quantitative yield. $LiBH_4$ reduction of both ester groups afforded **6a** in good yield.[19]

Compounds **6a** and **6b**[20] were converted to cyclic derivatives by exposure to paraformaldehyde and $BF_3 \cdot OEt_2$[21] to afford cyclic ethers **7a** and **7b** in 51% and 82% yield, respectively. Deprotection of compounds **7a** to **8a** was carried out by using n-$Bu_4N^+F^-$ in THF. Benzylether of **7b** was removed by a catalytic hydrogenation over 10% Pd−C to furnish **8b**. Mitsunobu inversion of the secondary hydroxyl groups of **8a**,**b** was accomplished by using *p*-nitrobenzoic acid, triphenylphosphine, and diisopropylazodicarboxylate in benzene at 23 °C. Saponification of the resulting esters provided **8c** and **8d**.

For the synthesis of compounds **8e** and **8f**, which represent the monoxygenated analogues of **8d**, a synthetic strategy based on a ring-closing metathesis reaction as the key step was planned (Schemes 2 and 3). Accordingly, secondary alcohol **9**[22] (Scheme

Scheme 1. Synthesis of Optically Active 1,3-Dioxacycloalkanes

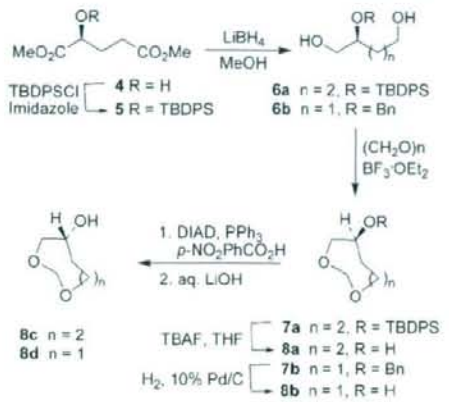

Scheme 2. Synthesis of Cyclic Ether **8e**

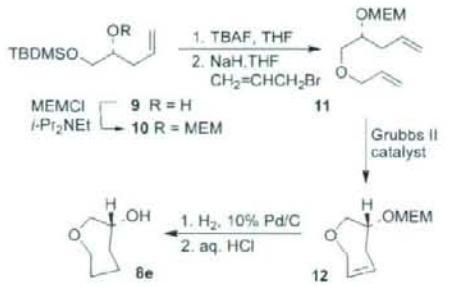

Scheme 3. Synthesis of Cyclic Ether **8f**

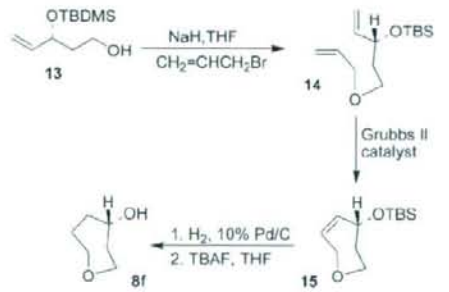

2) was protected as the corresponding methoxyethoxymethyl (MEM)-ether **10** in 90% yield using an excess of MEM-Cl in the presence of DIPEA in CH_2Cl_2.

Subsequent n-$Bu_4N^+F^-$-promoted deprotection of the TBDMS-group afforded the corresponding primary alcohol, which was treated with sodium hydride and alkylated with allyl bromide in the presence of a catalytic amount of n-$Bu_4N^+I^-$ to afford olefin **11** in 78% yield (2 steps). A 0.01 M solution of **11** in CH_2Cl_2 was then treated with a catalytic amount (5 mol%) of second generation Grubbs catalyst and heated to 45 °C to afford the cyclooxepane **12** in 94% yield. The double bond of **12** was finally reduced by catalytic hydrogenation using 10% Pd−C as the catalyst, and the MEM-ether was removed by acidic hydrolysis in a 1:1 THF/H_2O mixture to obtain the target alcohol **8e** in good overall yield.

For the synthesis of alcohol **8f** (Scheme 3), compound **13** was used as the starting material. It was in turn prepared following a described procedure starting from acrolein and *tert*-butylacetate.[23] Alkylation of the primary hydroxyl group of **13** with allyl bromide and n-$Bu_4N^+I^-$ using sodium hydride as the base furnished the ring closing metathesis precursor **14**. The cyclization reaction was performed by using second generation Grubbs catalyst (5 mol%) in CH_2Cl_2 and afforded olefin **15** in good yield. Subsequent hydrogenation of the double bond and n-$Bu_4N^+F^-$-mediated removal of TBDMS-ether finally afforded the target alcohol **8f**.

Scheme 4. Synthesis of Polyethers **8h−j**

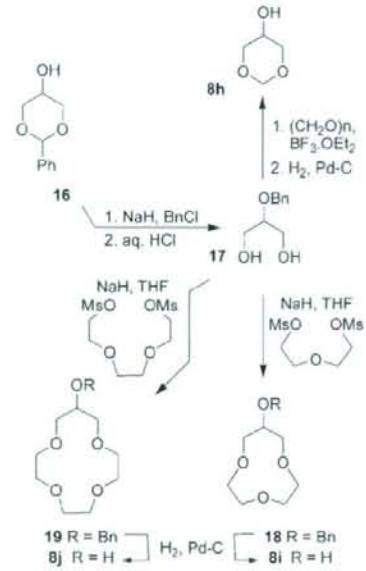

Alcohols **8h−j** required for the preparation of inhibitors **3h−j** were synthesized by starting from the common intermediate 2-benzyloxypropane-1,3-diol **17** as shown in Scheme 4. Compound **17** was prepared by alkylation of commercially available benzylidene acetal **16** with benzyl chloride in the presence of sodium hydride and a catalytic amount of n-$Bu_4N^+I^-$ in THF at 23 °C. The benzylidene group was subsequently removed by hydrolysis with 6 N HCl in a mixture (1:1) of THF and water to give 2-benzyloxy-1,3-propanediol **17** in quantitative yield. Treatment of **17** with paraformaldehyde and $BF_3\cdot OEt_2$ as described above, followed by hydrogenolysis of the resulting *O*-benzylether afforded **8h** in 78% overall yield.

Treatment of diol **17** with an excess of sodium hydride in refluxing THF followed by addition of di(ethyleneglycol)dimesylate or tri(ethyleneglycol)dimesylate afforded macrocycles **18** and **19** in 19% and 29% yield, respectively. Dilution of the reaction mixture to assist the intramolecular cyclization reaction did not result in a significant improvement of the reaction yields. Given the poor enzymatic inhibitory activity observed for the corresponding final compounds **3i** and **3j**, no further attempts were made to improve the cyclization yield for the preparation of these 10- and 13-membered polyether rings. Compounds **18** and **19** were subsequently deprotected by hydrogenolysis to obtain alcohols **8i** and **8j**.

We planned to investigate the effect of heteroatom functionalities in the polyether rings. In this context, we prepared the compounds **8k**, **8l**, and **24** from known diols **20**[24] as shown in Scheme 5. Thus, exposure of **20** to paraformaldehyde in the presence of $BF_3\cdot OEt_2$ furnished the corresponding cyclic